iScience

CellPress
OPEN ACCESS

Article

PTPσ Controls Presynaptic Organization of Neurotransmitter Release Machinery at Excitatory Synapses

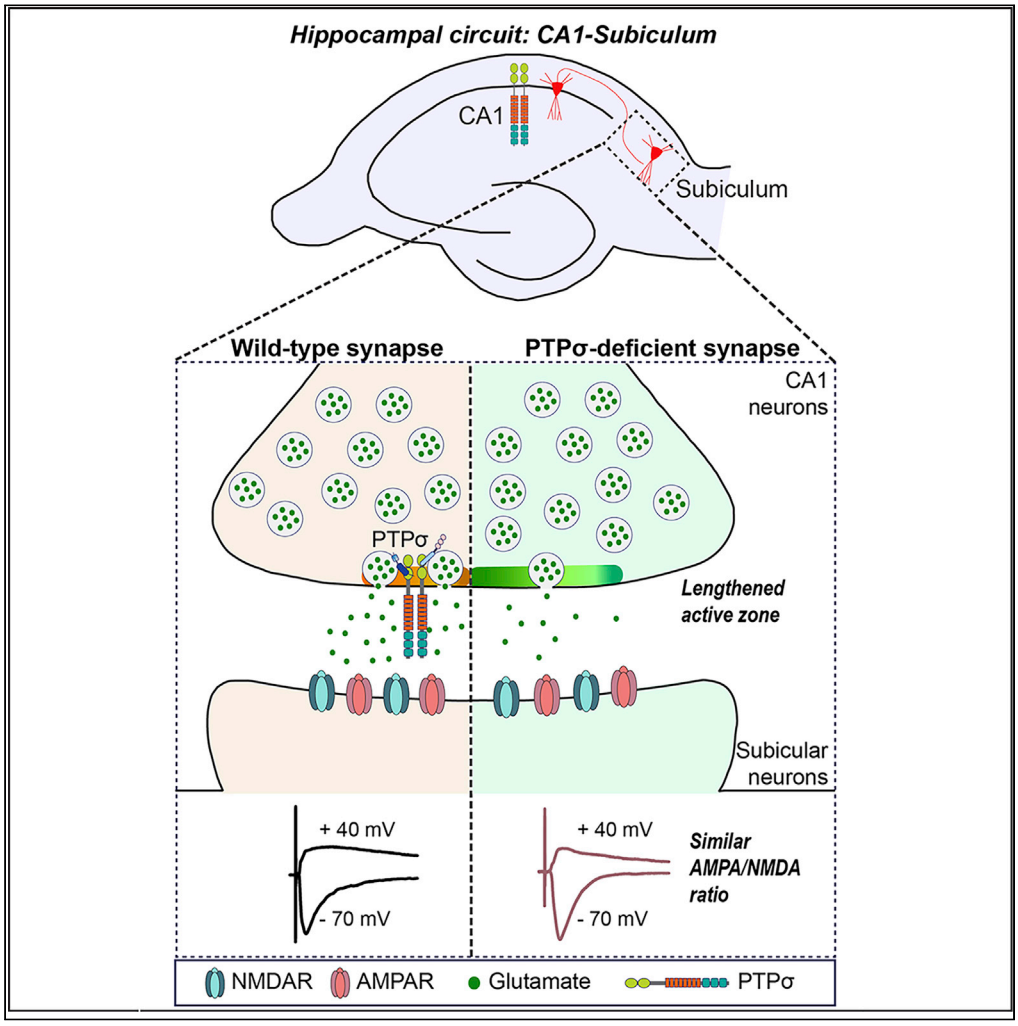

Kyung Ah Han, Hee-Yoon Lee, Dongseok Lim, ..., Ji Won Um, Se-Young Choi, Jaewon Ko

sychoi@snu.ac.kr (S.-Y.C.)
jaewonko@dgist.ac.kr (J.K.)

HIGHLIGHTS

Conditional PTPσ KO produces specifically impaired presynaptic functions

Presynaptic PTPσ regulates glutamate release efficiency

Presynaptic PTPσ does not transsynaptically regulate postsynaptic receptor responses

Han et al., iScience *23*, 101203
June 26, 2020
https://doi.org/10.1016/j.isci.2020.101203

iScience

CellPress
OPEN ACCESS

Article

PTPσ Controls Presynaptic Organization of Neurotransmitter Release Machinery at Excitatory Synapses

Kyung Ah Han,[1,2] Hee-Yoon Lee,[3] Dongseok Lim,[1] Jungsu Shin,[1] Taek Han Yoon,[1] Chooungku Lee,[4] Jeong-Seop Rhee,[4] Xinran Liu,[5] Ji Won Um,[1,2] Se-Young Choi,[3,6,*] and Jaewon Ko[1,6,7,*]

SUMMARY

Leukocyte common antigen-related receptor tyrosine phosphatases (LAR-RPTPs) are evolutionarily conserved presynaptic organizers. The synaptic role of vertebrate LAR-RPTPs *in vivo*, however, remains unclear. In the current study, we analyzed the synaptic role of PTPσ using newly generated, single conditional knockout (cKO) mice targeting PTPσ. We found that the number of synapses was reduced in PTPσ cKO cultured neurons in association with impaired excitatory synaptic transmission, abnormal vesicle localization, and abnormal synaptic ultrastructure. Strikingly, loss of presynaptic PTPσ reduced neurotransmitter release prominently at excitatory synapses, concomitant with drastic reductions in excitatory innervations onto postsynaptic target areas *in vivo*. Furthermore, loss of presynaptic PTPσ in hippocampal CA1 pyramidal neurons had no impact on postsynaptic glutamate receptor responses in subicular pyramidal neurons. Postsynaptic PTPσ deletion had no effect on excitatory synaptic strength. Taken together, these results demonstrate that PTPσ is a *bona fide* presynaptic adhesion molecule that controls neurotransmitter release and excitatory inputs.

INTRODUCTION

Distinct molecular assemblies at presynaptic nerve terminals and postsynaptic densities are responsible for the fast and precise transmission of neural information (Südhof, 2018). These structures act by coordinating the regulation of bidirectional signals across synaptic clefts, determining the properties of individual synapses, including the computation of neural information (Südhof, 2018). Several synaptic cell-adhesion molecules are thought to act not only as physical connectors across synaptic clefts but also as *trans*-synaptic signaling hubs (Missler et al., 2012; Südhof, 2017, 2018).

Leukocyte common antigen-related receptor tyrosine phosphatases (LAR-RPTPs) are evolutionarily conserved key synaptic organizers expressed in presynaptic active zones (AZs) (Han et al., 2019; Südhof, 2012; Um and Ko, 2013). Invertebrate LAR-RPTP orthologs (dLAR in *Drosophila melanogaster* and PTP-3 in *Caenorhabditis elegans*) were shown to be expressed in axons/growth cones, playing critical roles in axon guidance, dendritic growth, and synapse formation (Ackley et al., 2005; Chagnon et al., 2004; Han et al., 2019). In contrast, vertebrate LAR-RPTPs, consisting of three members (LAR, PTPσ, and PTPδ), are present in both dendritic spines and axons of cultured neurons (Han et al., 2018; Takahashi et al., 2012; Wyszynski et al., 2002). Analogous to Nrxns, LAR-RPTPs bind postsynaptic ligands, which do not overlap with Nrxn ligands, to induce presynaptic differentiation (Bomkamp et al., 2019; Choi et al., 2016; Han et al., 2018; Li et al., 2015; Takahashi et al., 2011; Yim et al., 2013; Yoshida et al., 2011). Constitutive KO mice of individual or multiple LAR-RPTP exhibit pleiotropic abnormalities in both the peripheral and central nervous systems and impairment in certain aspects of synapse development and function (Elchebly et al., 1999; Horn et al., 2012; McLean et al., 2002; Thompson et al., 2003; Uetani et al., 2000, 2006; Wallace et al., 1999). In contrast, loss of PTPσ and/or PTPδ, using short-hairpin-mediated knockdown (KD)-mediated manipulations, impairs structural and functional development, as well as the LAR-RPTP ligand-induced formation of artificial synapses (Bomkamp et al., 2019; Dunah et al., 2005; Han et al., 2018; Takahashi et al., 2012; Yim et al., 2013). Intriguingly, PTPσ and PTPδ serve as functional receptors for presynaptic assembly at specific synapse types (i.e., PTPσ for excitatory synapses, such as Slitrks, TrkC, and SALMs, and PTPδ for inhibitory synapses, such as Slitrk3, and excitatory synapses, such as IL1RAPL1) (Choi et al., 2016; Han et al., 2018; Li et al., 2015;

[1]Department of Brain and Cognitive Sciences, Daegu Gyeongbuk Institute of Science and Technology (DGIST), 333 Techno Jungangdae-Ro, Hyeonpoong-Eup, Dalseong-Gun, Daegu 42988, Korea

[2]Core Protein Resources Center, DGIST, 333 Techno Jungangdae-Ro, Hyeonpoong-Eup, Dalseong-Gun, Daegu 42988, Korea

[3]Department of Physiology and Neuroscience, Dental Research Institute, Seoul National University School of Dentistry, Seoul 03080, Korea

[4]Department of Molecular Neurobiology, Max Planck Institute of Experimental Medicine, Göttingen 37075, Germany

[5]Department of Cell Biology, Yale University School of Medicine, New Haven, CT 06510, USA

[6]Co-Senior Author

[7]Lead Contact

*Correspondence: sychoi@snu.ac.kr (S.-Y.C.), jaewonko@dgist.ac.kr (J.K.)

https://doi.org/10.1016/j.isci.2020.101203

Takahashi et al., 2012; Valnegri et al., 2011; Yim et al., 2013; Yoshida et al., 2011). Although these findings clearly indicated that LAR-RPTPs may be central components in both pre- and postsynaptic neurons that organize various aspects of synapse development, a sophisticated approach using conditional knockout (cKO) deficient in LAR-RPTPs is required to precisely assess the synaptic role of vertebrate LAR-RPTPs *in vivo*. A recent study showed that all three LAR-RPTPs regulate postsynaptic responses mediated by N-methyl-D-aspartate receptors (NMDA-type glutamate receptors) through *trans*-synaptic mechanism(s), but this study did not examine the presynaptic role of individual LAR-RPTPs (Sclip and Südhof, 2020).

In the present study, we generated mutant mice carrying PTPσ cKO alleles. We found that, in keeping with the KD effects (Han et al., 2018), conditional genetic deletions of PTPσ specifically impaired excitatory synaptic transmission. Moreover, deletion of PTPσ resulted in an abnormal vesicular organization in presynaptic boutons. Furthermore, PTPσ loss from hippocampal CA1 pyramidal neurons selectively impaired innervation and neurotransmitter release at excitatory, but not inhibitory, synapses formed on subicular pyramidal neurons. Strikingly, loss of presynaptic PTPσ in hippocampal CA1 neurons did not alter postsynaptic glutamate receptor-mediated responses in subicular neurons. These results suggest that PTPσ is essential for the regulation of presynaptic functions *in vivo*, distinct from the roles of presynaptic Nrxns.

RESULTS

Generation of PTPσ cKO Mice

Previous studies employing constitutive KO mice have precluded investigations of the mechanisms of action of LAR-RPTPs because of the pleiotropic phenotypes that are likely unrelated to their synaptic roles (Um and Ko, 2013). Transgenic mice with deletion of *PTPσ* were generated by crossing *PTPσ*$^{f/f}$ mice, with exon 4 flanked by *loxP* sites with a Cre recombinase driver line under control of the Nestin promoter (Nestin-Cre) (Figure S1). RNAscope-based fluorescence *in situ* hybridization showed that the expression patterns of mRNAs encoding all three LAR-RPTP family members overlap in both the mPFC and the hippocampus (Figure S2A). PTPσ and PTPδ mRNAs were detected in *CaMKIIα*-positive glutamatergic neurons and in *Gad1*-positive GABAergic neurons of adult mouse brains (Figures S2B and S2C).

To evaluate the cellular effects of endogenous PTPσ deletions, hippocampal neurons were cultured from PTPσ cKO mice. Neurons cultured for 3–4 days *in vitro* (DIV) were infected with lentiviruses expressing EGFP-fused nuclear Cre recombinase, which results in a global loss of PTPσ in all neurons due to high infection efficiency, or with a non-functional mutant version of Cre recombinase (ΔCre). Global expression of Cre recombinase caused a specific and nearly complete loss of PTPσ mRNA expression and completely eliminated PTPσ protein expression in PTPσ-cKO neurons analyzed at DIV13–14 (Figures S3A–S3C). Complete elimination of PTPσ protein was also confirmed by immunoblot analyses of lysates of PTPσ-cKO brains (Figure S3D). cKO mice in which PTPσ was deleted from the entire brain were viable and fertile, although a modest reduction of body size was observed (Figure S3E). In addition, PTPσ-cKO brains showed normal gross morphology, as revealed by staining for the neuron-specific marker NeuN (Figure S4A) and for Nissl (Figure S4B). Quantitative immunoblot analysis of PTPσ-deficient brains showed comparable expression of presynaptic AZ and postsynaptic density proteins (Figures S5A and S5B).

Conditional PTPσ KO Reduces the Number of Excitatory Synapses

To assess the synaptic role of PTPσ, cultured hippocampal PTPσ-cKO neurons were infected with lentiviruses expressing either ΔCre (Control) or wild-type Cre recombinase at DIV3–4 and the neurons were stained with antibodies to various excitatory and inhibitory synaptic markers at DIV14–16 (Figures 1A–1C). The density of excitatory, but not of inhibitory, synaptic puncta was significantly reduced, as measured by staining of PTPσ-deficient neurons with antibodies to GluA1 (both surface and total), pan-Shank, and VGLUT1 (~30%–40%) (Figures 1A and 1B). There were no marked changes in the density of inhibitory synaptic puncta on PTPσ KO neurons (Figures 1A and 1B). Moreover, measurements of the apparent sizes of synaptic puncta, reflecting a combination of antigen concentration and true synapse size, showed a small but significant reduction in the sizes of pan-Shank^{+} puncta on PTPσ-deficient neurons (Figures 1A and 1C). These results are consistent with the previously reported PTPσ KD effect (Han et al., 2018).

Conditional PTPσ KO Impairs Excitatory Synaptic Transmission

To examine whether the reduced number of synapses in PTPσ-deficient neurons were accompanied by corresponding effects on the transmission of respective synapse types, hippocampal dissociated cultured

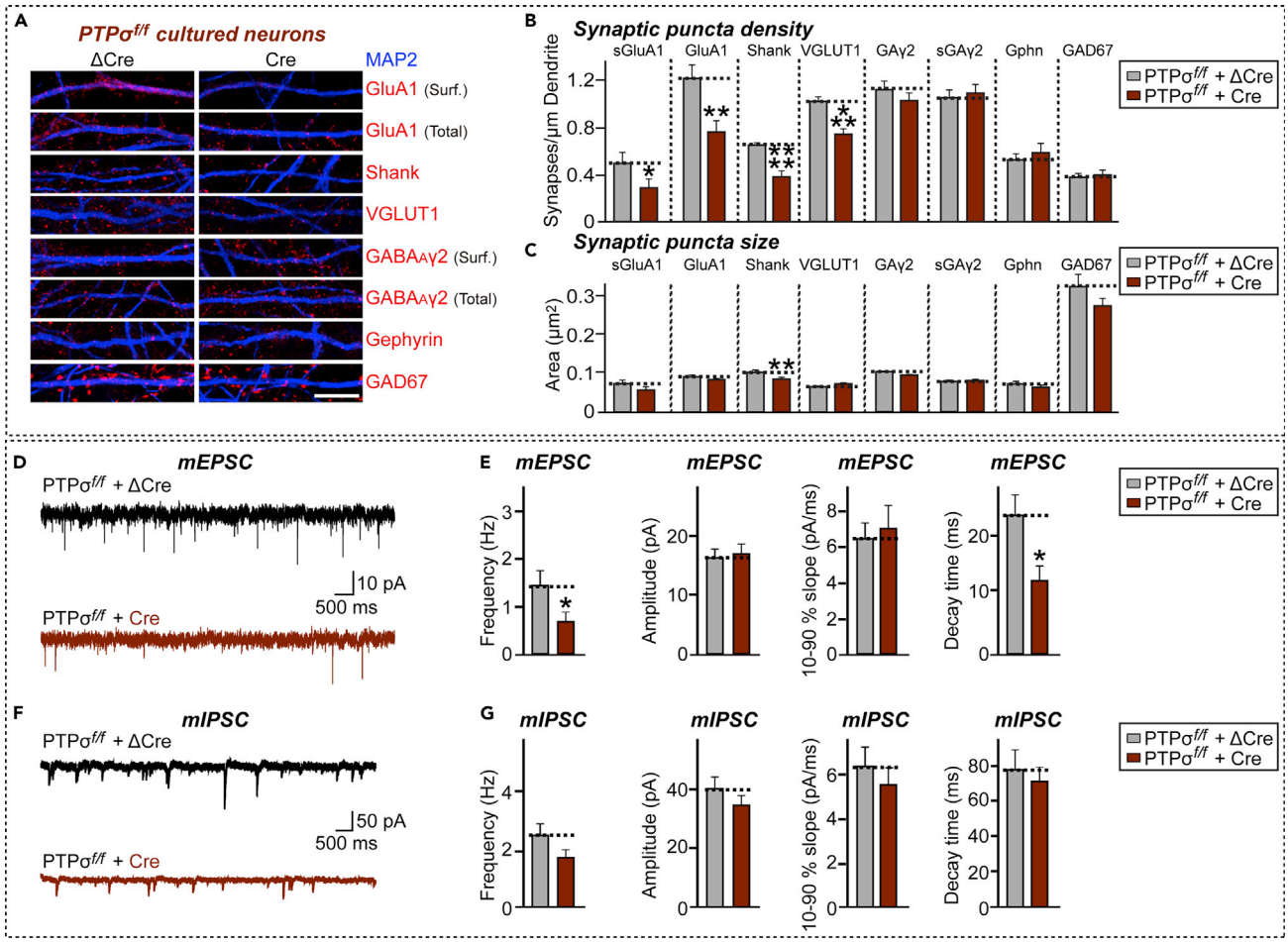

Figure 1. Conditional KO of PTPσ Impairs Excitatory Synapse Development and Transmission in Cultured Hippocampal Neurons

(A) PTPσ cKO in cultured hippocampal neurons specifically reduces excitatory synapse density. Double immunofluorescence analysis of MAP2 (blue) and the indicated synaptic markers (red) in mature cultured neurons (DIV14) derived from *PTPσ*$^{f/f}$ mice infected with lentiviruses expressing ΔCre or Cre at DIV3. Synaptic markers assayed included surface GluA1 (sGluA1), total GluA1, Shank, and VGLUT1 as excitatory synaptic markers, and surface $GABA_Aγ2$ (sGAγ2), total $GABA_Aγ2$, Gephyrin (Gphn), and GAD67 as inhibitory synaptic markers. Scale bar: 10 μm.

(B and C) Quantification of images in (A), measuring the density (B) and area (C) of the indicated synaptic marker puncta. Data are means ± SEMs (n denotes number of analyzed neurons; ΔCre/PTPσ cKO/sGluA1, n = 16; Cre/PTPσ cKO/sGluA1, n = 17; ΔCre/PTPσ cKO/GluA1, n = 16; Cre/PTPσ cKO/GluA1, n = 15; ΔCre/PTPσ cKO/Shank, n = 16; Cre/PTPσ cKO/Shank, n = 16; ΔCre/PTPσ cKO/VGLUT1, n = 15; Cre/PTPσ cKO/VGLUT1, n = 16; ΔCre/PTPσ cKO/sGABA$_A$Rγ2, n = 15; Cre/PTPσ cKO/sGABA$_A$Rγ2, n = 15; ΔCre/PTPσ cKO/GABA$_A$Rγ2, n = 16; Cre/PTPσ cKO/GABA$_A$Rγ2, n = 16; ΔCre/PTPσ cKO/Gephyrin, n = 16; Cre/PTPσ cKO/Gephyrin, n = 15; ΔCre/PTPσ cKO/GAD67, n = 16; and Cre/PTPσ cKO/GAD67, n = 16. Mann-Whitney U test; *p < 0.05; **p < 0.01; ***p < 0.001; ****p < 0.0001).

(D and E) Representative mEPSC traces (D) and quantification of frequencies, amplitudes, and kinetics (E) of mEPSCs recorded from hippocampal cultured neurons derived from *PTPσ*$^{f/f}$ mice infected with lentiviruses expressing inactive (ΔCre) or active (Cre) Cre recombinase. Data are means ± SEMs (n denotes number of analyzed neurons; ΔCre, 20 and Cre, 15; unpaired t test; *p < 0.05).

(F and G) Representative mIPSC traces (F) and quantification of frequencies, amplitudes, and kinetics (G) of mIPSCs recorded from hippocampal cultured neurons derived from *PTPσ*$^{f/f}$ mice infected with lentiviruses expressing ΔCre or Cre. Data are means ± SEMs (n denotes number of analyzed neurons; ΔCre, 18 and Cre, 17; unpaired t test)

neurons were assessed electrophysiologically (Figures 1D–1G). Lentivirus-mediated global loss of PTPσ specifically reduced the frequency (but not amplitude) of excitatory, but not inhibitory, synaptic transmission, as shown by measurement of miniature excitatory postsynaptic currents (mEPSCs) and miniature inhibitory postsynaptic currents (mIPSCs) (Figures 1E and 1G). These results are consistent with the PTPσ KD effect on excitatory synaptic transmission (Dunah et al., 2005; Han et al., 2018; Ko et al., 2015). Notably, PTPσ KO induced a significant decrease in mEPSC decay time (peak to 10%), implying a change in subunit composition of AMPA-type glutamate receptors (Jonas, 2000).

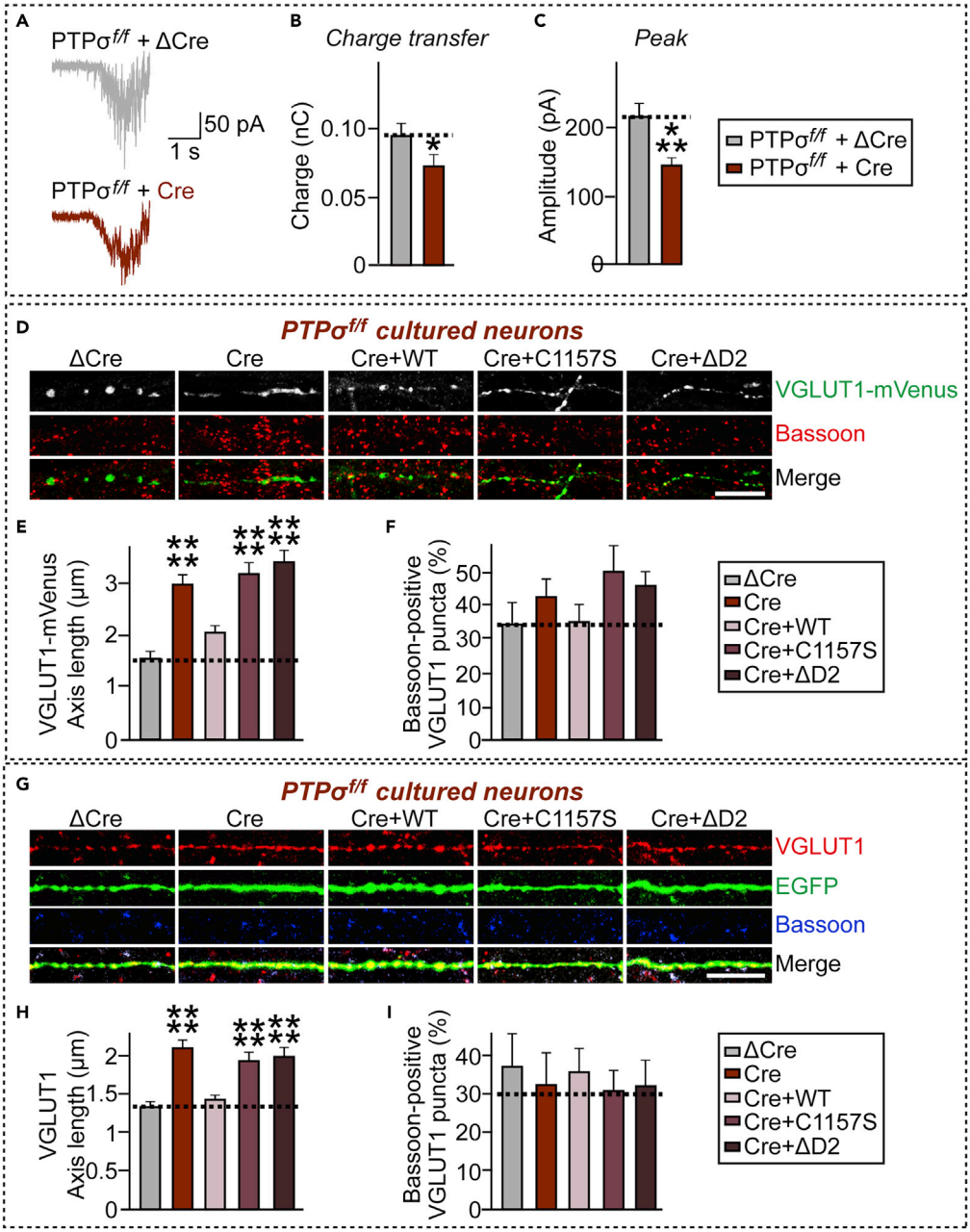

Figure 2. PTPσ Deletion Reduces Vesicle Localization in Excitatory Presynaptic Boutons

(A) Representative traces of AMPAR-EPSCs evoked by single 2-s pulse of 0.5 M sucrose delivered at a 1-min interval, recorded from hippocampal cultured neurons derived from *PTPσ*$^{f/f}$ mice infected with lentiviruses expressing inactive (ΔCre) or active (Cre) Cre recombinase.

(B and C) Bar graphs showing charge transfer (B) and peak amplitudes (C) of sucrose-evoked EPSCs, estimated as the synaptic charge transfer integrated over 30 s. Recordings were performed in the presence of 1 μM tetrodoxin and 50 μM picrotoxin. Data are means ± SEMs (n denotes number of analyzed neurons; ΔCre, 26 and Cre, 29; *p < 0.05; ***p < 0.001; unpaired t test).

(D) Representative images of cultured neurons (DIV10) derived from *PTPσ*$^{f/f}$ mice infected with lentiviruses expressing ΔCre or Cre at DIV3 and transfected with VGLUT1-mVenus (green) at DIV8. Anti-Bassoon (red) was used to mark the presynaptic active zone. Scale bar: 10 μm.

(E) Quantification of synaptic vesicle diffusion from images in (D), determined by measuring the average length of the major axis of VGLUT1-mVenus fluorescence in transfected axons. Data are means ± SEMs (n denotes the number of

Figure 2. *Continued*

analyzed neurons; ΔCre, n = 19; Cre, n = 18; Cre+/PTPσ WT, n = 15; Cre+/PTPσ C1157S, n = 15; and Cre+/PTPσ ΔD2, n = 17; ****p < 0.0001; ANOVA with a non-parametric Kruskal-Wallis test).

(F) Quantification of VGLUT1-mVenus fluorescence enrichment at presynaptic active zone for the images in (D). Data are means ± SEMs (n denotes the number of analyzed neurons; ΔCre, n = 19; Cre, n = 18; Cre+/PTPσ WT, n = 15; Cre+/PTPσ C1157S, n = 15; and Cre+/PTPσ ΔD2, n = 17; ANOVA with a non-parametric Kruskal-Wallis test).

(G) Representative images of cultured neurons (DIV10) derived from $PTP\sigma^{f/f}$ mice infected with lentiviruses expressing ΔCre or Cre at DIV3 and transfected with EGFP (green) at DIV8. Anti-Bassoon (blue) was used to mark the presynaptic active zone. Scale bar: 10 μm.

(H) Quantification of synaptic vesicle diffusion from images in (G), determined by measuring the average length of the major axis of VGLUT1 fluorescence in transfected axons. Data are means ± SEMs (n denotes the number of analyzed neurons; ΔCre, n = 14; Cre, n = 12; Cre+/PTPσ WT, n = 13; Cre+/PTPσ C1157S, n = 15; and Cre+/PTPσ ΔD2, n = 13; ****p < 0.0001; ANOVA with a non-parametric Kruskal-Wallis test).

(I) Quantification of VGLUT1 fluorescence enrichment at presynaptic active zone for the images in (G). Data are means ± SEMs (n denotes the number of analyzed neurons; ΔCre, n = 14; Cre, n = 12; Cre+/PTPσ WT, n = 13; Cre+/PTPσ C1157S, n = 15; and Cre+/PTPσ ΔD2, n = 13; ANOVA with a non-parametric Kruskal-Wallis test).

Conditional KO of PTPσ Reduces Synaptic Localization of Excitatory Synaptic Vesicles in Presynaptic Boutons

It is possible that deletion of PTPσ in presynaptic neurons alters localization of synaptic vesicles, resulting in reduced frequency of mEPSCs (Figure 1). Thus, we next asked whether PTPσ could regulate the size of readily releasable vesicles (RRPs) (Zucker and Regehr, 2002). We examined whether RRP size was changed at excitatory synapses by stimulating release of the entire RRP using a well-established hypertonic sucrose solution (500 mOsm) and quantifying RRP size by integrating the total charge transfer during the first 2 s of the release (Rosenmund and Stevens, 1996). Strikingly, the number of RRPs was significantly reduced in PTPσ-cKO neurons, as indicated by reductions of ~14.7% in charge transfer and ~31.2% in peak amplitude (Figures 2A–2C). This provides a hypothetical explanation for the positive regulation of neurotransmitter release by PTPσ at excitatory synapses.

To better understand the role of PTPσ in organizing presynaptic functions at the excitatory synapse (see Figure 1), we infected cultured hippocampal PTPσ-cKO neurons with ΔCre-EGFP or Cre-EGFP-expressing lentiviruses, transfected the neurons with mVenus-fused VGLUT1 (an excitatory synapse-specific vesicle marker) 5 days after the infections, and stained neurons with antibodies to Bassoon (a presynaptic AZ marker) 2 days after the transfections (Figures 2D–2F). We found that expression of VGLUT1-mVenus in PTPσ-cKO neurons resulted in a more diffuse pattern of mVenus-fused vesicular markers compared with control neurons infected with ΔCre-EGFP, indicating that ablation of PTPσ inhibits the synaptic localization of synaptic vesicles at excitatory presynaptic boutons (Figures 2D and 2E). No changes in Bassoon localization at presynaptic boutons were observed in PTPσ-cKO neurons (Figures 2D, 2F, and 2I). To further dissect the mechanism by which PTPσ regulates vesicle localization at excitatory synapses, we designed three lentiviruses expressing PTPσ variants, based on validated HA epitope-tagged PTPσ variants that were previously used in cultured neurons (Han et al., 2018). These lentiviruses expressed PTPσ wild-type (WT), a PTPσ deletion mutant lacking the D2 domain (ΔD2), or a PTPσ point mutant defective in tyrosine phosphatase activity (C1157S). Lentiviral expression of PTPσ WT, but not other PTPσ variants, completely reversed the diffuse distribution pattern of VGLUT1-mVenus fluorescence (Figures 2D and 2E) and puncta immunoreactive to anti-VGLUT1 antibodies (Figures 2G and 2H) in PTPσ-cKO neurons, producing a punctate pattern. In addition, synaptic localization of vesicles was not rescued by expression of PTPσ intracellular mutants, suggesting that PTPσ requires D2 domain-mediated molecular interactions and tyrosine phosphatase activity to appropriately direct excitatory synaptic vesicles into presynaptic boutons. Collectively, these results suggest that PTPσ is involved in presynaptic assembly by organizing vesicle localization at excitatory synapses using intracellular mechanisms.

Conditional KO of PTPσ Alters Active Zone Architectures

To further understand whether PTPσ-cKO affects synaptic structures, we examined presynaptic terminals and postsynaptic densities in cultured cells and imaged chemically fixed hippocampal neurons using transmission electron microscopy (TEM), as previously described (Acuna et al., 2016) (Figure 3). TEM analyses of cultured neurons showed that PTPσ-deficient and control presynaptic terminals contained similar numbers of total vesicles (Figures 3A and 3D). Surprisingly, AZ length was increased by ~30% (Figures 3A and 3B), similar to the doubling in AZ size in *Caenorhabditis elegans* mutants lacking *ptp-3A*, an ortholog of the type

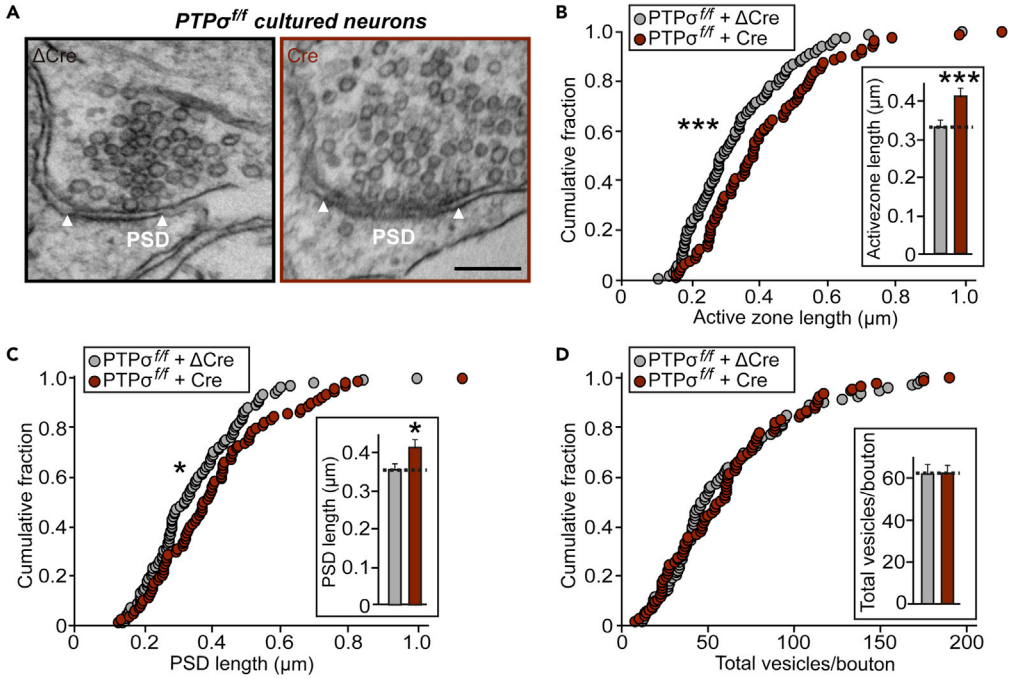

Figure 3. PTPσ Deletion Induces Abnormal Organization of Synaptic Structures

(A) Representative electron micrographs of hippocampal neurons cultured from *PTPσ*$^{f/f}$ mice infected with lentiviruses expressing ΔCre (control) or Cre.

(B and C) PTPσ deletion increases length of synaptic membranes. Cumulative distribution of the lengths of AZ (B) and PSD (C) for the indicated genotypes. Data are means ± SEMs (n denotes the number of analyzed neurons; ΔCre, 100 and Cre, 88; *p < 0.05; ***p < 0.001; Mann-Whitney U test).

(D) Total numbers of vesicles per bouton in control and PTPσ-deficient synapses. Data are means ± SEMs (n denotes the number of analyzed neurons; ΔCre, 100 and Cre, 88).

IIa RPTP gene (Ackley et al., 2005; Han et al., 2019). Consistent with this, a corresponding increase (~15%) in PSD length was observed (Figures 3A and 3C). These results suggest that PTPσ is crucial in controlling the structural organization of both presynaptic AZs and PSDs.

Conditional PTPσ KO in CA1 Neurons Reduces Excitatory Presynaptic Innervation onto Postsynaptic Subicular Neurons and Excitatory Neurotransmitter Release

Although the synaptic roles of invertebrate orthologs of type IIa RPTPs have been primarily studied from the perspective of their presynaptic structure and function (Chagnon et al., 2004; Um and Ko, 2013), PTPσ appears to be expressed at both presynaptic and postsynaptic neurons (Dunah et al., 2005; Han et al., 2018) (Figure S5C). Because the functional locus of a specific synaptic protein cannot be precisely determined in cultured neurons, a Cre driver line under the control of a Wolfram syndrome 1 homolog (Wfs1) promoter was utilized (Kitamura et al., 2014; Madisen et al., 2010). The presence of Wfs1-positive neurons, including in the dorsal CA1 and layer II/III of the mPFC, was confirmed by robust tdTomato expression in the Ai9 reporter mouse line (Luuk et al., 2008; Madisen et al., 2010) (Figure S6A). Immunohistochemical analysis of Wfs1 expression in the mPFC and hippocampal CA1 showed strong Wfs1-immunoreactive signals in Tbr1-positive excitatory neurons but not GAD67-positive GABAergic neurons (Figure S6B). Thus, Wfs1-*PTPσ* mice (obtained by crossing *PTPσ*$^{f/f}$ mice with a Wfs1-Cre driver line) allowed us to investigate the effects of selective loss of PTPσ at presynaptic loci in a given neural circuit. The pre- and postsynaptic effects of PTPσ deletions were analyzed by focusing on presynaptic CA1 neurons of the hippocampus at synapses formed onto postsynaptic pyramidal neurons in the subiculum. Wfs1-*PTPσ* mice were viable and fertile and comparable in size with control mice (Figure S6C). Moreover, NeuN and Nissl staining of Wfs1-*PTPσ* brains showed normal gross morphology (Figures S6D and S6E). Anatomical changes at synapses formed by presynaptic CA1 region neurons on postsynaptic subicular neurons were evaluated by quantitative immunofluorescence analyses (Figure 4A), which showed that the density and integrated intensity of VGLUT1 puncta were significantly reduced in subicular neurons (Figures 4B–4D). However, the density and intensity of GAD67 puncta in the corresponding brain regions were comparable in Wfs1-*PTPσ* and control mice (Figures

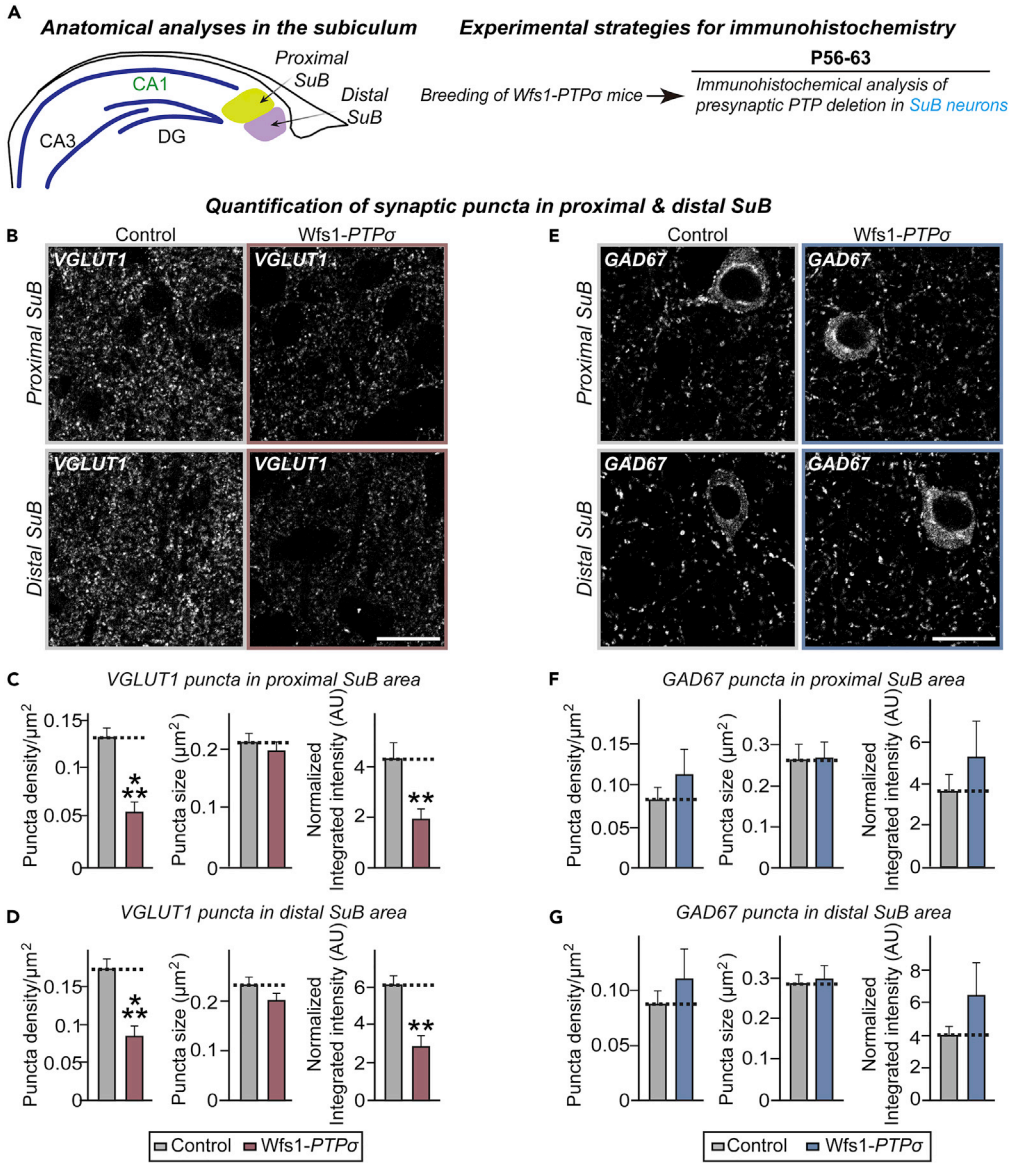

Figure 4. Wfs1-*PTPσ* KO Mice Exhibit Decreased Excitatory Synaptic Innervation in Postsynaptic Subicular Pyramidal Neurons

(A) Schematic depiction of anatomical analyses in the subiculum. Each subiculum was divided into the proximal and distal subiculum.

(B and E) Representative immunofluorescence images of the proximal and distal SuB of Control and Wfs1-*PTPσ* mice using VGLUT1 (B) or GAD67 (E). Scale bar: 20 μm.

(C and F) Quantification of the density, size, and integrated intensity of VGLUT1-positive (C) and GAD67-positive (F) synaptic puncta in the proximal SuB. Data are means ± SEMs (n denotes the number of analyzed brain mice; 8 mice per group; **p < 0.01 and ***p < 0.001; Mann-Whitney U test).

(D and G) Quantification of the density, size, and integrated intensity of VGLUT1-positive (D) and GAD67-positive (G) synaptic puncta in the distal SuB. Data are means ± SEMs (n denotes the number of analyzed mice; 8 mice per group; **p < 0.01, ***p < 0.001; Mann-Whitney U test). See also Figures S7 and S8.

4E–4G). Adeno-associated viruses (AAVs) expressing Cre recombinase (AAV-Cre) or inactive Cre recombinase (AAV-ΔCre) were stereotactically injected into ventral hippocampal CA1 (vCA1) of $PTP\sigma^{f/f}$ mice. Subsequent quantitative immunohistochemical analyses showed decreased excitatory (but not GABAergic) innervations onto subicular neurons from $PTP\sigma^{f/f}$ mice infected with AAV-Cre (Figure S7).

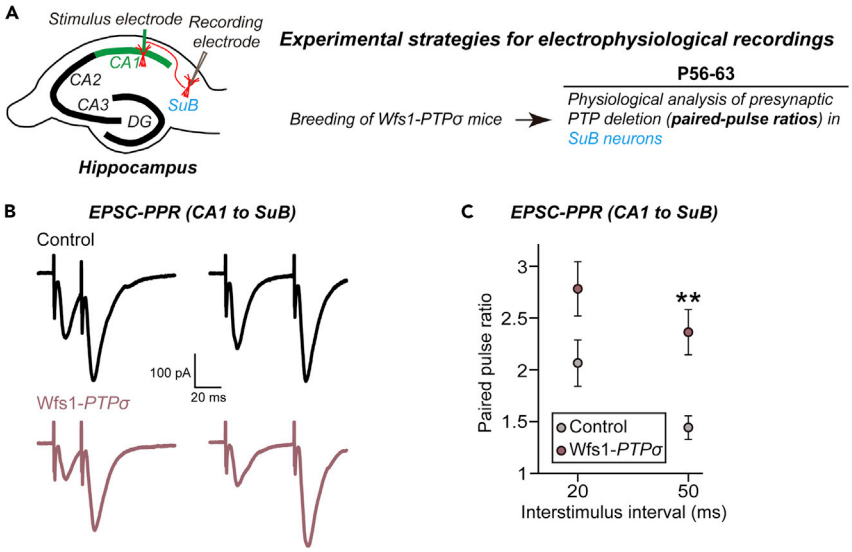

Figure 5. Presynaptic Deletion of PTPσ Impairs Neurotransmitter Release at Excitatory Synapses of Postsynaptic Subicular Pyramidal Neurons

(A) Experimental strategies for electrophysiological recordings in hippocampal SuB neurons of Wfs1-*PTPσ* mice.

(B) Representative traces of paired pulse ratios (PPRs) of EPSCs in synapses of CA1–SuB at two different interstimulus intervals (20 and 50 ms for EPSC-PPRs).

(C) EPSC-PPRs in synapses of CA1–SuB as a function of the indicated interstimulus intervals. Data are means ± SEMs (**$p < 0.01$; two-tailed Student's t test).

To further corroborate these anatomical observations and identify any possible presynaptic changes, PPRs in subicular neurons were measured (Figure 5A). EPSC-PPRs were significantly increased in hippocampal CA1-to-subicular synapses (Figures 5B and 5C). Taken together, these results suggest that PTPσ is a critical modulator of presynaptic innervations and neurotransmitter release at excitatory synapses.

Conditional PTPσ Deletions Exert No Postsynaptic Effect

Next, the effect of presynaptic deletion of PTPσ on basal synaptic transmission was analyzed in Wfs1-*PTPσ* mice. Unexpectedly, there was a no reduction in frequency or amplitude of spontaneous EPSCs (sEPSCs) in subicular pyramidal neurons (Figures S8A–S8C). A recent study using triple conditional KO mice lacking all three LAR-RPTPs showed decreased NMDA receptor-mediated responses in hippocampal CA1 neurons (Sclip and Südhof, 2020). Thus, we tested whether PTPσ deletion also regulated postsynaptic responses via a *trans*-synaptic mechanism. To test this, we assessed the ratio of AMPA- to NMDA-receptor mediated EPSCs (i.e., AMPA/NMDA ratio) by stimulating Schaffer collateral axons of hippocampal CA3 neurons or axons of hippocampal CA1 neurons and measuring postsynaptic responses in hippocampal CA1 neurons or subicular neurons (Figures 6 and 7). There was no change in the AMPA/NMDA ratio at PTPσ-deficient CA1 pyramidal neurons or subicular neurons innervated by PTPσ-deficient CA1 pyramidal neurons (Figures 6 and 7). In addition, there was no change in the frequency or amplitude of mEPSCs in PTPσ-deficient CA1 pyramidal neurons (Figure S8). These results suggest that PTPσ primarily functions presynaptically and does not *trans*-synaptically regulate postsynaptic responses *in vivo*.

DISCUSSION

Prior investigations using constitutive KO mice lacking one or two LAR-RPTPs, or shRNA-mediated KD approaches, showed that LAR-RPTPs are significant regulators of various aspects of nervous system development (Chagnon et al., 2004; Han et al., 2016, 2019; Takahashi and Craig, 2013; Um and Ko, 2013). These studies showed that LAR-RPTPs affect the development and/or maturation of synapses as well as have potential compensatory adaptations and possibly unintentional off-target phenomena during development. Therefore, the present study involved the generation of PTPσ floxed mice, with these conditional KO mice analyzed to determine the synaptic roles of PTPσ. Our *in vitro* data demonstrated that PTPσ KO specifically reduced the numbers of excitatory synapses and basal excitatory synaptic transmission, in agreement with previous KD studies (Han et al., 2018; Ko et al., 2015) (Figure 1). Moreover, PTPσ KO decreased RRP size and

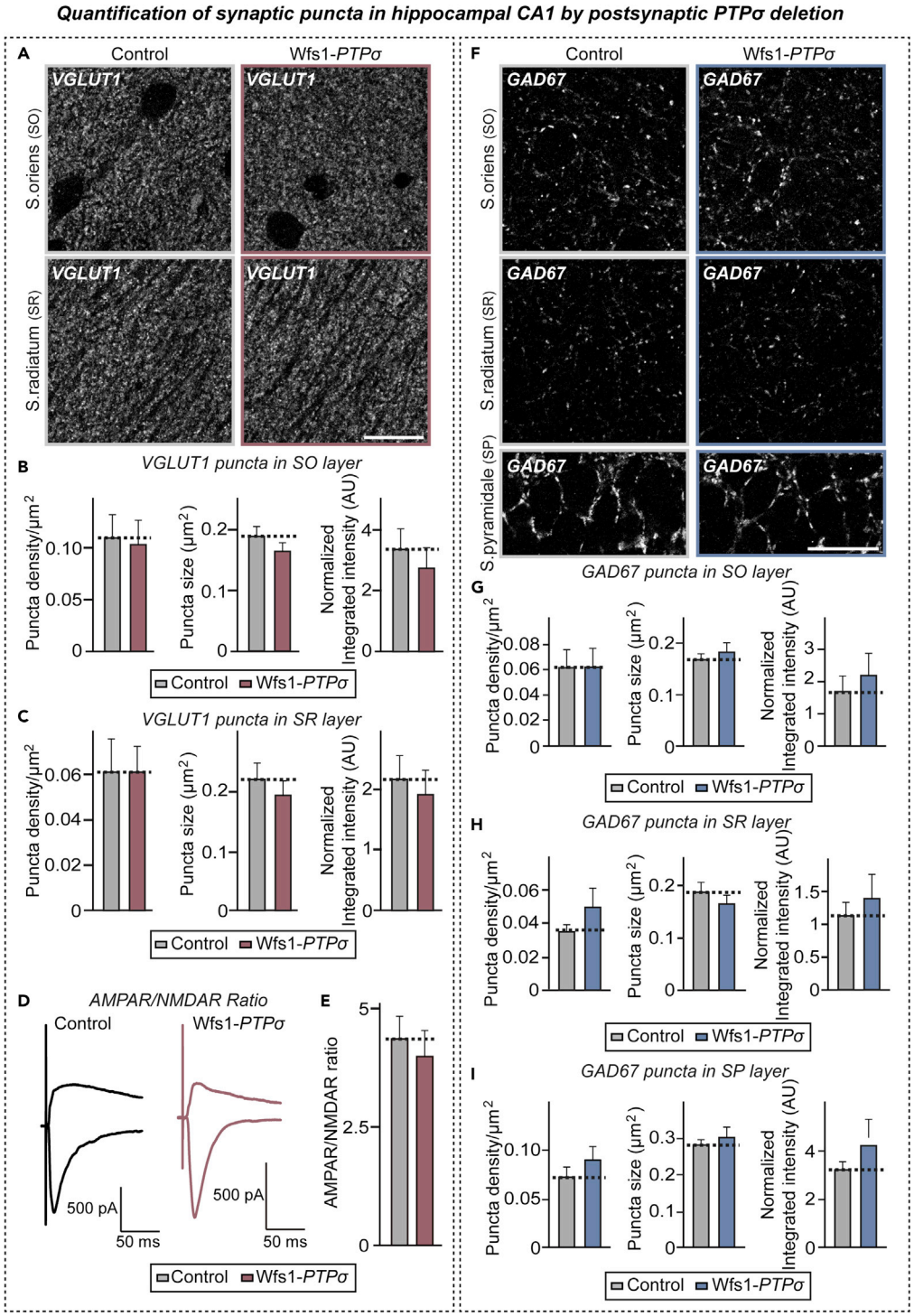

Figure 6. Postsynaptic Deletion of PTPσ Exerts No Effects on Excitatory Synapse Organization in Hippocampal CA1 Region

(A and F) Representative immunofluorescence images of the *stratum oriens* (SO) and *stratum pyramidal* (SP) layer of control and Wfs1-*PTPσ* mice using VGLUT1 (A) or GAD67 (F). Scale bar: 20 μm.

(B and C) Quantification of the density, size, and integrated intensity of VGLUT1-positive synaptic puncta in the SO (B) and SR (C) layers of the hippocampal CA1 region. Data are means ± SEMs (n = 8 mice per group; Mann-Whitney U test).

(D) Representative traces of evoked EPSCs at holding potentials of −70 and +40 mV in control and Wfs1-*PTPσ* mice.

Figure 6. *Continued*
(E) AMPAR/NMDAR ratios at CA3–CA1 synapses, calculated by dividing the EPSC peak amplitude at 10 ms (−70 mV) by the EPSC amplitude at 130 ms (+40 mV). Data are means ± SEMs (n = 14 cells from 4–5 mice; two-tailed Student's t test). (G–I) Quantification of the density, size, and integrated intensity of GAD67-positive synaptic puncta in the SO (G), SR (H), and SP (I) layers of the hippocampal CA1 region. Data are means ± SEM (n = 8 mice per group; Mann-Whitney U test).

synaptic localization of excitatory synaptic vesicles (Figure 2). Furthermore, PTPσ KO altered ultrastructural features (Figure 3). Our *in vivo* results further suggest that PTPσ functions presynaptically at excitatory synapses involving hippocampal CA1–subiculum connections in the hippocampus by modulating glutamate release (Figures 4 and 5). Compared with the pervasive loss-of-function consequences of Nrxns in various cell types across diverse brain areas and neural circuits (Südhof, 2017), the effects of conditional deletion of PTPσ were relatively marginal. These findings were unexpected, as members of the LAR-RPTP family bind to various synapse organizers crucial for discrete aspects of synapse development (Südhof, 2017; Um and Ko, 2013).

A rich body of previous studies have shown that invertebrate LAR-RPTPs have presynaptic roles in controlling AZ assembly and proper vesicle localization (Han et al., 2019). A few studies of vertebrate LAR-RPTP function have revealed their critical roles in postsynaptic neurons, including their regulation of spine morphogenesis development and their stabilization of surface AMPA-type glutamate receptors (Dunah et al., 2005; Wyszynski et al., 2002). Because several LAR-RPTP ligands have been identified as putative postsynaptic organizers in rodent neurons, LAR-RPTPs were thought to act in presynaptic neurons in a manner similar to Nrxns (Südhof, 2012). Taken together with our previous results (Han et al., 2018), our current findings demonstrate that PTPσ KO and PTPσ KD have similar overall effects on synapse density and transmission *in vitro*, indicating the importance of confirmatory analyses using a sophisticated system and approaches in elucidating PTPσ function *in vivo*. It is possible, however, that the approaches employed in this study were not sufficiently sensitive to detect subtle changes in synapse properties. Moreover, the selection of experimental preparations may preclude detection of synaptic roles of PTPσ at *in vivo* synapses. In addition, PTPδ may functionally compensate for PTPσ loss, but not *vice versa*, whereas PTPσ may have peripheral roles in the operation of specific neural circuits in which PTPδ is expressed. The use of cKO models to study the canonical and non-canonical roles of PTPσ *in vivo* at various stages of synapse development in other classes of neurons is warranted and may provide a more sophisticated understanding of how LAR-RPTPs act as a multivalent signaling platform in presynaptic neurons.

Our results suggest that PTPσ contributes to the organization of *trans*-synaptic nanomolecular complexes for efficient glutamate release (Figure 6). Investigation of common/redundant functions of LAR-RPTPs using conditional triple KOs of PTPσ, PTPδ, and LAR is required to provide further insights into the major observations of the current study (Sclip and Südhof, 2020). In addition, it remains to be determined whether LAR-RPTPs and other presynaptic adhesion molecules (e.g., Nrxns) cooperate in the presynaptic assembly *in vivo* (Roppongi et al., 2020).

Impaired glutamate release efficiency observed in PTPσ cKO mice has been observed in several prior studies reporting loss of function of Nrxn1α (Etherton et al., 2009), liprin-α2 (Spangler et al., 2013), and RIM1 (Kaeser et al., 2008). PTPσ KO drastically suppressed RRP size in cultured neurons that is controlled by positional priming (Neher and Sakaba, 2008) (Figure 2). These results suggest that PTPσ KO may disorganize AZ structure (Figure 3) and function by decoupling key nanomolecular machinery in AZs, a possibility that remains to be tested using high-resolution imaging or electron microscopy analyses.

Our genetic manipulations using the Wfs1-Cre driver line allowed determination of the presynaptic or postsynaptic role of PTPσ in excitatory neurons (Figures 4–7). PTPσ deletion in hippocampal CA1 reduced structural innervation of excitatory inputs and increased EPSC-PPRs in subicular neurons, without changing the frequency or amplitude of sEPSCs (Figures 5 and S8). Intriguingly, PTPσ deletion in hippocampal CA1 failed to elicit any changes in Schaffer collateral evoked excitatory synaptic transmission or basal synaptic transmission, indicating that PTPσ is not involved in *trans*-synaptic regulation of postsynaptic responses in the hippocampal CA1-subicular synapses *in vivo*. Given that deletion of all three LAR-RPTPs significantly decreases postsynaptic NMDA-type receptor responses in hippocampal Schaffer collateral neural circuits (Sclip and Südhof, 2020), it is possible that PTPδ and LAR might be selectively involved in controlling

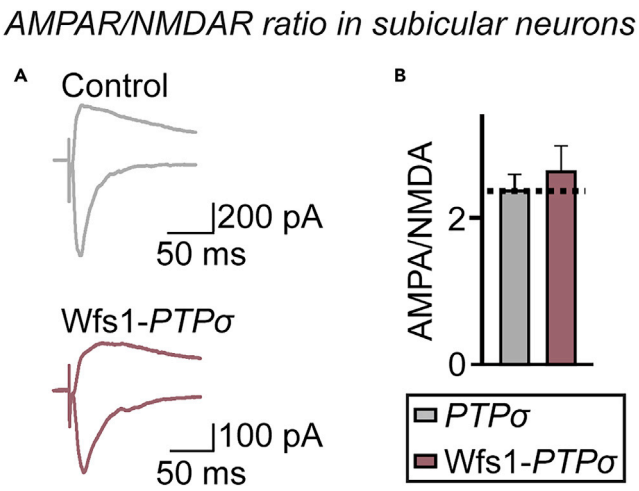

Figure 7. Presynaptic Deletion of PTPσ in Hippocampal CA1 Area Exerts No Altered Postsynaptic Responses in Subicular Neurons

(A) Representative traces of evoked EPSCs at holding potentials of −70 and +40 mV in control and Wfs1-*PTPσ* mice.
(B) AMPAR/NMDAR ratios at CA1–Sub synapses, calculated by dividing the EPSC peak amplitude at 10 ms (−70 mV) by the EPSC amplitude at 130 ms (+40 mV). Data are means ± SEMs (n denotes the number of analyzed neurons; Control, 15 cells/4 mice and Wfs1-*PTPσ*, 12 cells/4 mice; two-tailed Student's t test).

this synapse property in hippocampal CA1-subicular synapses. It is equally likely that LAR-RPTPs specifically regulate postsynaptic NMDA-type receptor responses in only a subset of neural circuits (i.e., CA3-CA1 synapses). It is also worth addressing whether alterations in AMPA-type glutamate receptor subunit composition occur *in vivo* at synapses of PTPσ-deficient neurons and, if so, what their significance might be. Future studies are warranted to systematically address these possibilities. In sum, our results clearly demonstrate that PTPσ is a key presynaptic factor in tuning presynaptic properties by organizing the neurotransmitter release machinery at excitatory synapses.

Limitations of the Study

Although the current study clearly demonstrated a presynaptic role for PTPσ in regulating neurotransmitter release at hippocampal CA1-subicular synapses, it remains to be determined whether this role extends generally to other hippocampal neural circuits and circuits in other brain areas. In addition, it is unclear how PTPσ and other LAR-RPTP members (PTPδ and LAR) exert their differential canonical functions in presynaptic neurons. Furthermore, differences in the requirement for PTPσ in controlling postsynaptic responses at different hippocampal synapses need to be more rigorously probed. Lastly, the pathological significance and mechanisms of coupling of PTPσ (and by extension, LAR-RPTPs) to intracellular machineries warrant further systematic investigation.

Resource Availability

Lead Contact

Further information and requests for resources and reagents should be directed to and will be fulfilled by Jaewon Ko (jaewonko@dgist.ac.kr)

Materials Availability

All unique/stable reagents generated in this study are available from the Lead Contact upon reasonable request and with a completed Materials Transfer Agreement.

Data and Code Availability

This study did not generate datasets.

METHODS

All methods can be found in the accompanying Transparent Methods supplemental file.

SUPPLEMENTAL INFORMATION

Supplemental Information can be found online at https://doi.org/10.1016/j.isci.2020.101203.

ACKNOWLEDGMENTS

We thank Jinha Kim (DGIST) for her technical assistance, Drs. Susumu Tonegawa (MIT, USA) and Albert Chen (DUKE-NUS, Singapore) for the gift of Wfs1-Cre and Nestin-Cre driver lines, respectively. This study was supported by grants from the Korea Healthcare Technology R & D Project, funded by the Ministry for Health and Welfare Affairs, Republic of Korea (Grant HI17C0080 to J.K.) and the National Research Foundation of Korea (NRF), funded by the Ministry of Science and ICT (2019R1A2B5B02069324 to J.K.).

AUTHOR CONTRIBUTIONS

S.-Y.C. and J.K. conceived the project; K.A.H., H.-Y.L., D.L., J.S., T.H.Y., C.L., and X.L. performed the experiments; K.A.H., H.-Y.L., D.L., J.S., T.H.Y., C.L., J.-S.R., J.W.U., S.-Y.C., and J.K. analyzed the data; S.-Y.C. and J.K. wrote the manuscript with input from the other authors.

DECLARATION OF INTERESTS

The authors declare no competing interests.

Received: March 3, 2020
Revised: May 4, 2020
Accepted: May 22, 2020
Published: June 26, 2020

REFERENCES

Ackley, B.D., Harrington, R.J., Hudson, M.L., Williams, L., Kenyon, C.J., Chisholm, A.D., and Jin, Y. (2005). The two isoforms of the *Caenorhabditis elegans* leukocyte-common antigen related receptor tyrosine phosphatase PTP-3 function independently in axon guidance and synapse formation. J. Neurosci. *25*, 7517–7528.

Acuna, C., Liu, X., and Südhof, T.C. (2016). How to make an active zone: unexpected universal functional redundancy between RIMs and RIM-BPs. Neuron *91*, 792–807.

Bomkamp, C., Padmanabhan, N., Karimi, B., Ge, Y., Chao, J.T., Loewen, C.J.R., Siddiqui, T.J., and Craig, A.M. (2019). Mechanisms of PTPsigma-mediated presynaptic differentiation. Front. Synaptic Neurosci. *11*, 17.

Chagnon, M.J., Uetani, N., and Tremblay, M.L. (2004). Functional significance of the LAR receptor protein tyrosine phosphatase family in development and diseases. Biochem. Cell Biol. *82*, 664–675.

Choi, Y., Nam, J., Whitcomb, D.J., Song, Y.S., Kim, D., Jeon, S., Um, J.W., Lee, S.G., Woo, J., Kwon, S.K., et al. (2016). SALM5 trans-synaptically interacts with LAR-RPTPs in a splicing-dependent manner to regulate synapse development. Sci. Rep. *6*, 26676.

Dunah, A.W., Hueske, E., Wyszynski, M., Hoogenraad, C.C., Jaworski, J., Pak, D.T., Simonetta, A., Liu, G., and Sheng, M. (2005). LAR receptor protein tyrosine phosphatases in the development and maintenance of excitatory synapses. Nat. Neurosci. *8*, 458–467.

Elchebly, M., Wagner, J., Kennedy, T.E., Lanctot, C., Michaliszyn, E., Itie, A., Drouin, J., and Tremblay, M.L. (1999). Neuroendocrine dysplasia in mice lacking protein tyrosine phosphatase sigma. Nat. Genet. *21*, 330–333.

Etherton, M.R., Blaiss, C.A., Powell, C.M., and Südhof, T.C. (2009). Mouse neurexin-1alpha deletion causes correlated electrophysiological and behavioral changes consistent with cognitive impairments. Proc. Natl. Acad. Sci. U S A *106*, 17998–18003.

Han, K.A., Jeon, S., Um, J.W., and Ko, J. (2016). Emergent synapse organizers: LAR-RPTPs and their companions. Int. Rev. Cell. Mol. Biol. *324*, 39–65.

Han, K.A., Ko, J.S., Pramanik, G., Kim, J.Y., Tabuchi, K., Um, J.W., and Ko, J. (2018). PTPsigma drives excitatory presynaptic assembly via various extracellular and intracellular mechanisms. J. Neurosci. *38*, 6700–6721.

Han, K.A., Um, J.W., and Ko, J. (2019). Intracellular protein complexes involved in synapse assembly in presynaptic neurons. Adv. Protein Chem. Struct. Biol. *116*, 347–373.

Horn, K.E., Xu, B., Gobert, D., Hamam, B.N., Thompson, K.M., Wu, C.L., Bouchard, J.F., Uetani, N., Racine, R.J., Tremblay, M.L., et al. (2012). Receptor protein tyrosine phosphatase sigma regulates synapse structure, function and plasticity. J. Neurochem. *122*, 147–161.

Jonas, P. (2000). The time course of signaling at central glutamatergic synapses. News Physiol. Sci. *15*, 83–89.

Kaeser, P.S., Kwon, H.B., Chiu, C.Q., Deng, L., Castillo, P.E., and Südhof, T.C. (2008). RIM1alpha and RIM1beta are synthesized from distinct promoters of the RIM1 gene to mediate differential but overlapping synaptic functions. J. Neurosci. *28*, 13435–13447.

Kitamura, T., Pignatelli, M., Suh, J., Kohara, K., Yoshiki, A., Abe, K., and Tonegawa, S. (2014). Island cells control temporal association memory. Science *343*, 896–901.

Ko, J.S., Pramanik, G., Um, J.W., Shim, J.S., Lee, D., Kim, K.H., Chung, G.Y., Condomitti, G., Kim, H.M., Kim, H., et al. (2015). PTPsigma functions as a presynaptic receptor for the glypican-4/LRRTM4 complex and is essential for excitatory synaptic transmission. Proc. Natl. Acad. Sci. U S A *112*, 1874–1879.

Li, Y., Zhang, P., Choi, T.Y., Park, S.K., Park, H., Lee, E.J., Lee, D., Roh, J.D., Mah, W., Kim, R., et al. (2015). Splicing-Dependent trans-synaptic SALM3-LAR-RPTP interactions regulate excitatory synapse development and locomotion. Cell Rep. *12*, 1618–1630.

Luuk, H., Koks, S., Plaas, M., Hannibal, J., Rehfeld, J.F., and Vasar, E. (2008). Distribution of Wfs1 protein in the central nervous system of the mouse and its relation to clinical symptoms of the Wolfram syndrome. J. Comp. Neurol. *509*, 642–660.

Madisen, L., Zwingman, T.A., Sunkin, S.M., Oh, S.W., Zariwala, H.A., Gu, H., Ng, L.L., Palmiter, R.D., Hawrylycz, M.J., Jones, A.R., et al. (2010). A robust and high-throughput Cre reporting and characterization system for the whole mouse brain. Nat. Neurosci. *13*, 133–140.

McLean, J., Batt, J., Doering, L.C., Rotin, D., and Bain, J.R. (2002). Enhanced rate of nerve regeneration and directional errors after sciatic nerve injury in receptor protein tyrosine

phosphatase sigma knock-out mice. J. Neurosci. *22*, 5481–5491.

Missler, M., Südhof, T.C., and Biederer, T. (2012). Synaptic cell adhesion. Cold Spring Harb. Perspect. Biol. *4*, a005694.

Neher, E., and Sakaba, T. (2008). Multiple roles of calcium ions in the regulation of neurotransmitter release. Neuron *59*, 861–872.

Roppongi, R.T., Dhume, S.H., Padmanabhan, N., Silwal, P., Zahra, N., Karimi, B., Bomkamp, C., Patil, C.S., Champagne-Jorgensen, K., Twiley, R.E., et al. (2020). Neuron *106*, 108–125.

Rosenmund, C., and Stevens, C.F. (1996). Definition of the readily releasable pool of vesicles at hippocampal synapses. Neuron *16*, 1197–1207.

Sclip, A., and Südhof, T.C. (2020). LAR receptor phospho-tyrosine phosphatases regulate NMDA-receptor responses. Elife *9*, e53406.

Spangler, S.A., Schmitz, S.K., Kevenaar, J.T., de Graaff, E., de Wit, H., Demmers, J., Toonen, R.F., and Hoogenraad, C.C. (2013). Liprin-alpha2 promotes the presynaptic recruitment and turnover of RIM1/CASK to facilitate synaptic transmission. J. Cell Biol. *201*, 915–928.

Südhof, T.C. (2012). The presynaptic active zone. Neuron *75*, 11–25.

Südhof, T.C. (2017). Synaptic neurexin complexes: a molecular code for the logic of neural circuits. Cell *171*, 745–769.

Südhof, T.C. (2018). Towards an understanding of synapse formation. Neuron *100*, 276–293.

Takahashi, H., and Craig, A.M. (2013). Protein tyrosine phosphatases PTPdelta, PTPsigma, and LAR: presynaptic hubs for synapse organization. Trends Neurosci. *36*, 522–534.

Takahashi, H., Arstikaitis, P., Prasad, T., Bartlett, T.E., Wang, Y.T., Murphy, T.H., and Craig, A.M. (2011). Postsynaptic TrkC and presynaptic PTPsigma function as a bidirectional excitatory synaptic organizing complex. Neuron *69*, 287–303.

Takahashi, H., Katayama, K., Sohya, K., Miyamoto, H., Prasad, T., Matsumoto, Y., Ota, M., Yasuda, H., Tsumoto, T., Aruga, J., and Craig, A.M. (2012). Selective control of inhibitory synapse development by Slitrk3-PTPdelta trans-synaptic interaction. Nat. Neurosci. *15*, 389–398.

Thompson, K.M., Uetani, N., Manitt, C., Elchebly, M., Tremblay, M.L., and Kennedy, T.E. (2003). Receptor protein tyrosine phosphatase sigma inhibits axonal regeneration and the rate of axon extension. Mol. Cell. Neurosci. *23*, 681–692.

Uetani, N., Kato, K., Ogura, H., Mizuno, K., Kawano, K., Mikoshiba, K., Yakura, H., Asano, M., and Iwakura, Y. (2000). Impaired learning with enhanced hippocampal long-term potentiation in PTPdelta-deficient mice. EMBO J. *19*, 2775–2785.

Uetani, N., Chagnon, M.J., Kennedy, T.E., Iwakura, Y., and Tremblay, M.L. (2006). Mammalian motoneuron axon targeting requires receptor protein tyrosine phosphatases sigma and delta. J. Neurosci. *26*, 5872–5880.

Um, J.W., and Ko, J. (2013). LAR-RPTPs: synaptic adhesion molecules that shape synapse development. Trends Cell Biol. *23*, 465–475.

Valnegri, P., Montrasio, C., Brambilla, D., Ko, J., Passafaro, M., and Sala, C. (2011). The X-linked intellectual disability protein IL1RAPL1 regulates excitatory synapse formation by binding PTPdelta and RhoGAP2. Hum. Mol. Genet. *20*, 4797–4809.

Wallace, M.J., Batt, J., Fladd, C.A., Henderson, J.T., Skarnes, W., and Rotin, D. (1999). Neuronal defects and posterior pituitary hypoplasia in mice lacking the receptor tyrosine phosphatase PTPsigma. Nat. Genet. *21*, 334–338.

Wyszynski, M., Kim, E., Dunah, A.W., Passafaro, M., Valtschanoff, J.G., Serra-Pages, C., Streuli, M., Weinberg, R.J., and Sheng, M. (2002). Interaction between GRIP and liprin-alpha/SYD2 is required for AMPA receptor targeting. Neuron *34*, 39–52.

Yim, Y.S., Kwon, Y., Nam, J., Yoon, H.I., Lee, K., Kim, D.G., Kim, E., Kim, C.H., and Ko, J. (2013). Slitrks control excitatory and inhibitory synapse formation with LAR receptor protein tyrosine phosphatases. Proc. Natl. Acad. Sci. U S A *110*, 4057–4062.

Yoshida, T., Yasumura, M., Uemura, T., Lee, S.J., Ra, M., Taguchi, R., Iwakura, Y., and Mishina, M. (2011). IL-1 receptor accessory protein-like 1 associated with mental retardation and autism mediates synapse formation by trans-synaptic interaction with protein tyrosine phosphatase delta. J. Neurosci. *31*, 13485–13499.

Zucker, R.S., and Regehr, W.G. (2002). Short-term synaptic plasticity. Annu. Rev. Physiol. *64*, 355–405.

iScience, Volume *23*

Supplemental Information

PTPσ Controls Presynaptic Organization of Neurotransmitter Release Machinery at Excitatory Synapses

Kyung Ah Han, Hee-Yoon Lee, Dongseok Lim, Jungsu Shin, Taek Han Yoon, Chooungku Lee, Jeong-Seop Rhee, Xinran Liu, Ji Won Um, Se-Young Choi, and Jaewon Ko

SUPPLEMENTAL FIGURES

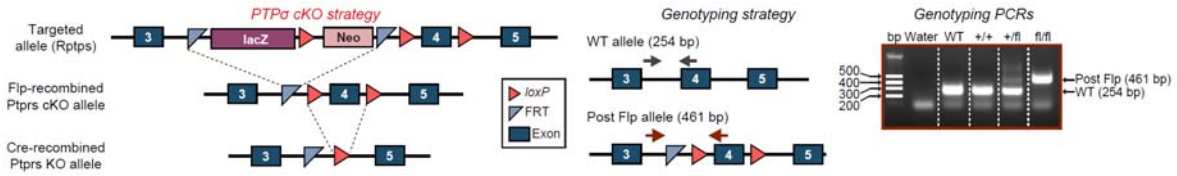

Supplemental Figure S1. Generation of PTPσ floxed Mice. Related to *All Figures*.

Conditional KO (cKO) strategy for PTPσ mouse lines. Exon 4 of the PTPσ gene was targeted (left). Primer locations for the WT and post Flp alleles are indicated with arrows (middle). PCR genotyping of WT and PTPσ floxed mice (right).

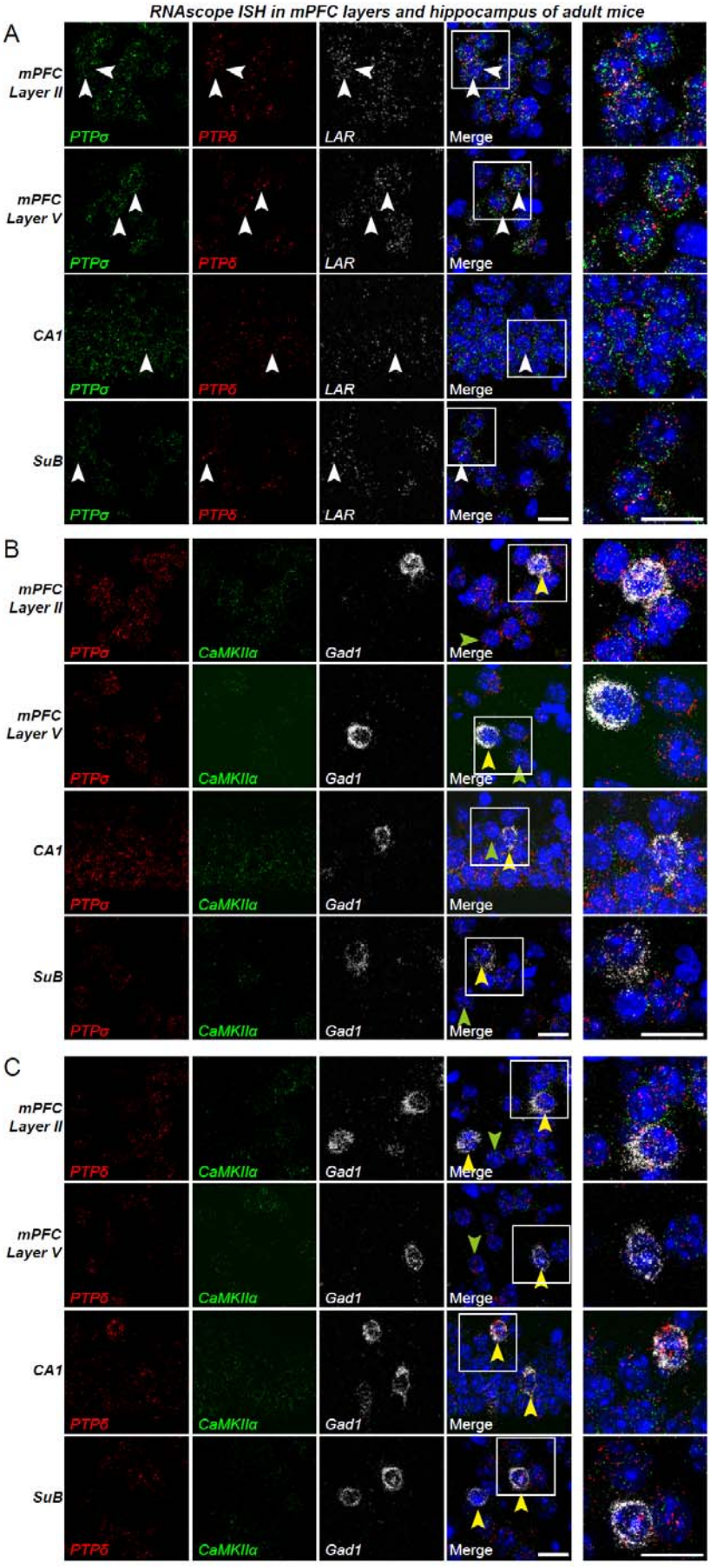
RNAscope ISH in mPFC layers and hippocampus of adult mice
A
mPFC Layer II
mPFC Layer V
CA1
SuB
PTPσ
PTPδ
LAR
Merge
B
CaMKIIα
Gad1
C

Supplemental Figure S2. Detection of LAR-RPTP mRNAs in Both Glutamatergic and GABAergic Neurons of Adult Mouse Brain. Related to *All Figures.*

(**A**) Representative high-resolution image of adult mouse brain regions (PFC layer II, mPFC layer V, hippocampal CA1, and SuB) visualized with probes targeting PTPσ (green), PTPδ (red) and LAR (white), and counterstained with DAPI (blue). White arrows indicate neurons with single cells expressing PTPσ, PTPδ and LAR mRNAs. Images (boxed in the merged image) on the right side are enlarged to clearly show quadruple labeling at the single-cell level. Scale bar, 20 μm.

(**B**) Representative high-resolution image of the indicated mouse brain regions, showing expression of PTPσ (red) in CaMKIIα-positive pyramidal neurons (green) and Gad1-positive GABAergic interneurons (white). Images (boxed in the merged image) on the right side are enlarged to clearly show quadruple labeling at the single-cell level. Scale bar, 20 μm.

(**C**) Representative high-resolution image of the indicated mouse brain region, showing expression of PTPδ (red) in CaMKIIα-positive pyramidal neurons (green) and Gad1-positive GABAergic interneurons (white). Images (boxed in the merged image) on the right side are enlarged to clearly show quadruple labeling at the single-cell level. Scale bar, 20 μm.

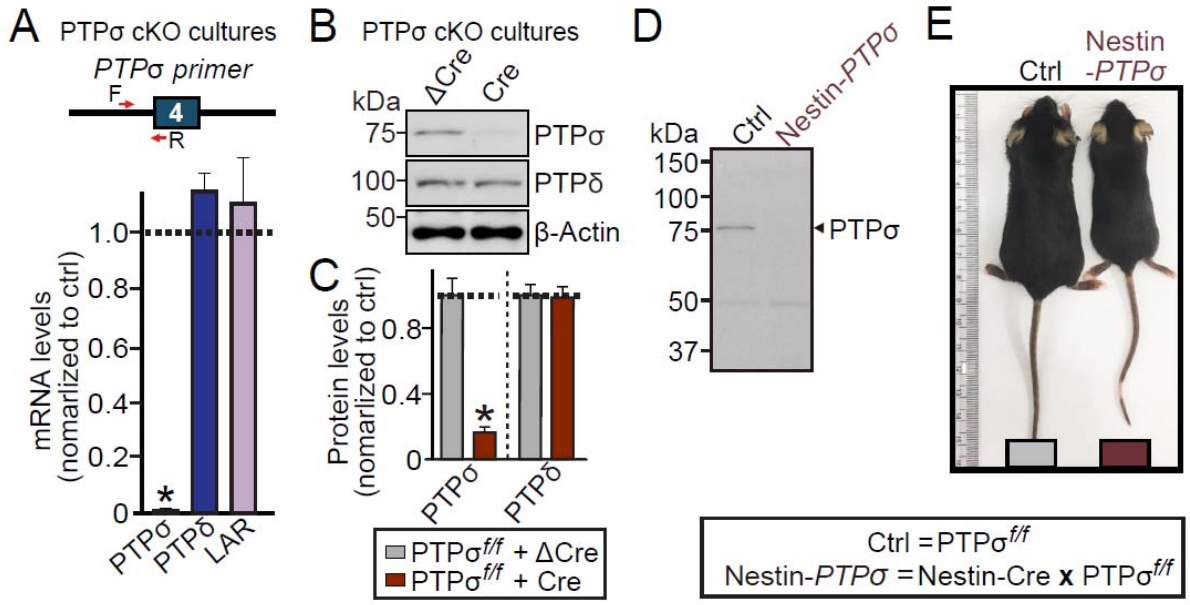

Supplemental Figure S3. Validation of PTPσ cKO Mice. Related to *All Figures*.

(**A**) Quantitative RT-PCR analysis of neuron RNA. Relative levels of PTPσ, PTPδ, and LAR mRNAs were measured in cultured cortical neurons infected with lentiviruses expressing Cre-recombinase. Data are means ± SEMs (n = 4 independent experiments).

(**B and C**) Representative immunoblot image (**B**) and quantitative analysis (**C**) of PTPσ protein in cultured cortical neurons infected with lentiviruses expressing Cre recombinase. β-actin was used as a loading control. Data are means ± SEMs (n = 4 independent experiments).

(**D**) Representative immunoblot analysis of level of PTPσ protein in brain homogenates from 8-week old control and PTPσ cKO mice. Levels of PTPσ protein was measured in the PTPσ floxed mice crossed with *Nestin-Cre* mice (Nestin-*PTPσ*) or respective PTP floxed mice (Ctrl). Arrows indicate band(s) immunoreactive with PTPσ-specific antibody.

(**E**) Images illustrating the body size of littermate control (Ctrl), Nestin-*PTPσ* mouse at 2 months of age. Nestin-*PTPσ* mouse was significantly smaller than age- and sex-matched Ctrl mice.

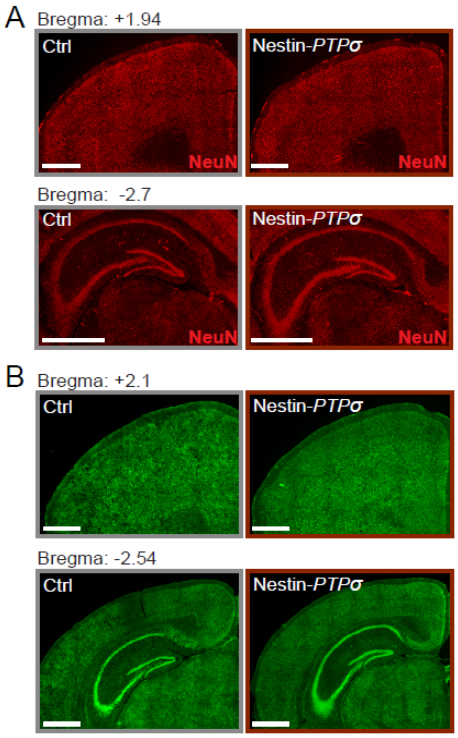

Supplemental Figure S4. Intact Cytoarchitecture in Conditional PTPσ KO Mice. Related to *All Figures.*

(**A**) Representative images of NeuN staining. Brain sections from *PTPσ*$^{f/f}$ (Ctrl) and Nestin-PTPσ mice were stained with the neuronal marker NeuN (red). Scale bar: 1 mm.

(**B**) Representative images of Nissl staining. Brain sections from *PTPσ*$^{f/f}$ (Ctrl) mice and from Nestin-PTPσ mice stained with NeuroTrace™ 500/525 Green Fluorescent Nissl Stain solution (green). Scale bar: 1 mm.

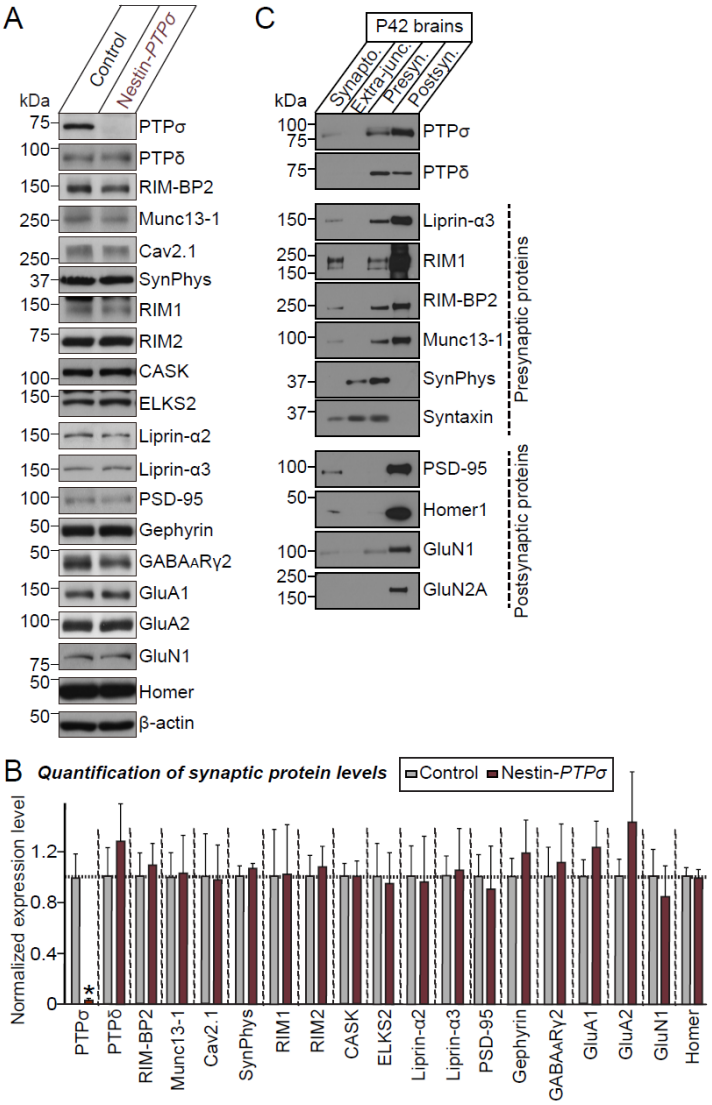

Supplemental Figure S5. Quantitative Immunoblot Analyses of PTPσ-deficient Mouse Brains. Related to *All Figures*.

(**A**) Representative images of immunoblot analysis using brain lysates from Nestin-*PTPσ* mice (n = 4 mice per group).

(**B**) Quantitative immunoblot analysis of PTPs, AZ proteins, and PSD proteins from control and Nestin-*PTPσ* mice. Data are means ± SEMs (n = 4 mice per group).

(**C**) Representative immunoblots of crude synaptosome (Synapto.), extrasynaptic junction (Extra-junc.), presynaptic (Presyn.), and postsynaptic (Postsyn.) fractions of adult mouse

brains. Both PTPσ and PTPδ were present at pre- and postsynaptic sites. Presynaptic active zone proteins and postsynaptic proteins were analyzed in parallel immunoblots.

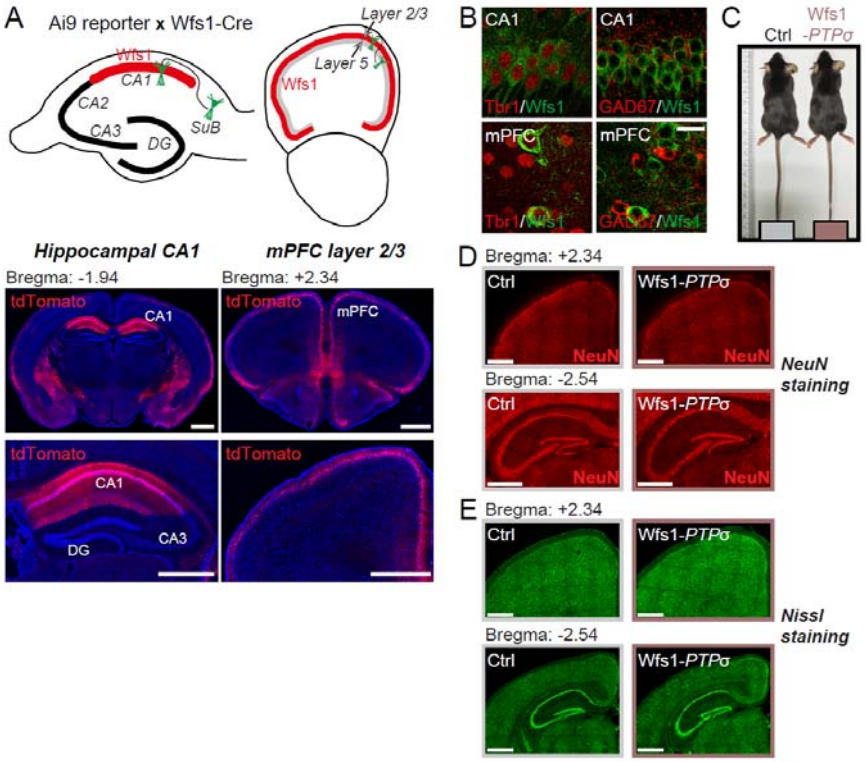

Supplemental Figure S6. Generation and Characterization of Wfs1-PTPσ KO Mice. Related to *Figures 4, 5, 6 & 7*.

(**A**) Schematic diagram (upper panel) and representative images (lower panel) of mice from the Wfs1-Cre driver line intercrossed with Ai9 reporter mice. tdTomato-positive neurons (red) in the hippocampal CA1 and layer II/III of the medial prefrontal cortex (mPFC) were detected by immunofluorescence analysis. Scale bar: 1 mm.

(**B**) Immunolocalization of Wfs1 protein (green) in mPFC and the hippocampal CA1 region of adult mice. Double immunofluorescence analysis for Tbr1 (red) and GAD67 (red) showed robust expression of Wfs1 in Tbr1-positive pyramidal neurons, but not in GAD67-positive inhibitory neurons. Scale bar: 20 μm.

(**C**) Images illustrating the body size of *PTPσ*$^{f/f}$ (Ctrl) and Wfs1-*PTPσ* littermates at 7 weeks of age. Body sizes of age- and sex-matched Ctrl and Wfs1-PTPσ mice were similar.

(**D**) Representative images of brain sections from *PTPσ*$^{f/f}$ (Ctrl) and Wfs1-*PTPσ* mice stained

with the neuronal marker NeuN (red). Scale bar: 1 mm.

(**E**) Representative images of brain sections from *PTPσ*$^{f/f}$ (Ctrl) and Wfs1-*PTPσ* mice stained with NeuroTrace™ 500/525 Green Fluorescent Nissl Stain solution (green). Scale bar: 1 mm.

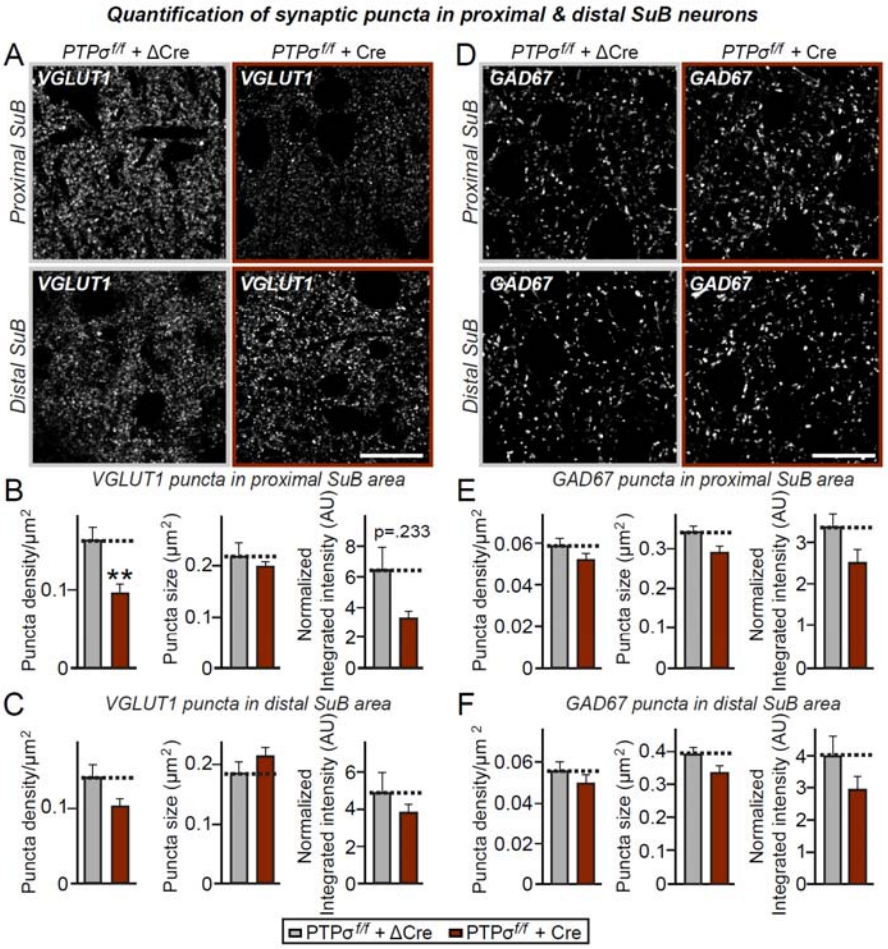

Supplemental Figure S7. Deletion of PTPσ from Hippocampal CA1 Specifically Decreases Innervation of Excitatory Synaptic Inputs on Subicular neurons. Related to *Figure 4*.

(**A, D**) Representative VGLUT1 (**A**) and GAD67 (**D**) positive immunofluorescence images of proximal and distal SuB of *PTPσ*$^{f/f}$ mice injected with AAV-ΔCre or AAV-Cre. Scale bar: 20 µm.

(**B, E**) Quantification of the density, size and integrated intensity of VGLUT1-positive (**B**) and GAD67-positive (**E**) synaptic puncta in proximal SuB. Data are means ± SEMs (n denotes the number of analyzed brain slices; 18–19 brain slices from 4 mice; $^{**}p < 0.01$; Mann Whitney U-test).

(**C, F**) Quantification of the density, size and integrated intensity of VGLUT1-positive (**C**) and GAD67-positive (**F**) synaptic puncta in distal SuB. Data are means ± SEMs (n denotes the number of analyzed brain slices; 18–19 brain slices from 4 mice; Mann Whitney U-test).

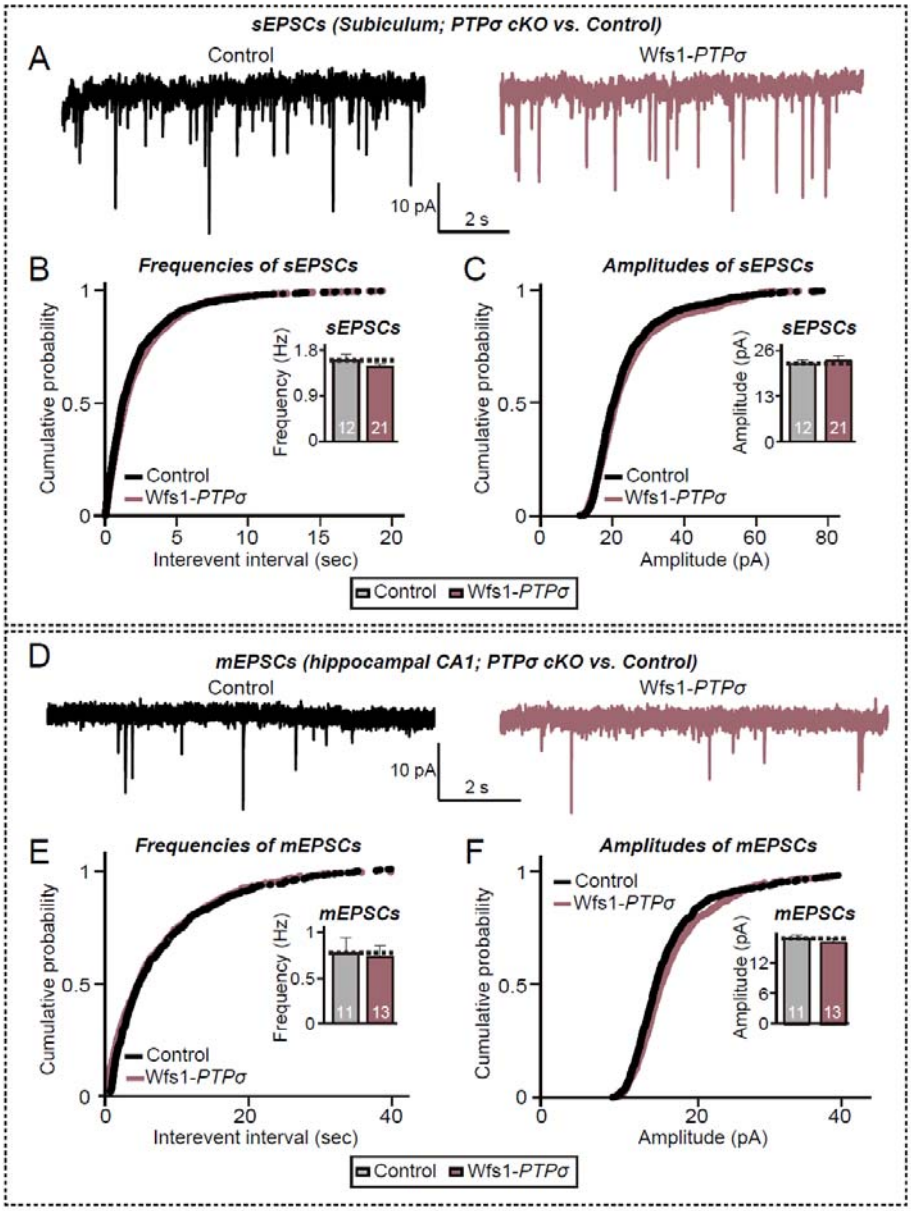

Supplemental Figure S8. Marginal Effect of Presynaptic Deletion of PTPσ on Excitatory and Inhibitory Synaptic Transmission in Pyramidal Neurons of Hippocampal Subiculum. Related to *Figure 4*.

(**A–C**) Representative sEPSC traces (**A**) recorded from SuB pyramidal neurons in acute SuB slices from littermate control and Wfs1-*PTPσ* mice, and cumulative distribution of sEPSC frequencies (**B**) and amplitudes (**C**). Insets show average sEPSC frequencies (**B**) and

amplitudes (**C**). Data are means ± SEMs (n denotes the number of analyzed neurons; Control, 12; and Wfs1-PTPσ, 21; two-tailed Student's t-tests).

(**D–F**) Representative mEPSC traces (**D**) recorded from CA1 pyramidal neurons in acute CA1 slices from littermate control and Wfs1-*PTPσ* mice, and cumulative distribution plots of mEPSC frequencies (**E**) and amplitudes (**F**). Insets show average mEPSC frequencies (**E**) and amplitudes (**F**). Data are means ± SEMs (n denotes the number of analyzed neurons; Control, 11; and Wfs1-*PTPσ*, 13; two-tailed Student's t-tests).

TRANSPARENT METHODS

KEY RESOURCES TABLE

REAGENT or RESOURCE	SOURCE	IDENTIFIER
Antibodies		
Mouse monoclonal Anti-PTPσ	MediMabs	Cat #MM-0020; RRID: AB_1808357
Mouse monoclonal Anti-GAD67	Millipore	Cat #MAB5406; RRID: AB_2278725
Rabbit polyclonal Anti-VGLUT1	Synaptic Systems	Cat #135 311; RRID: AB_887880
Guinea pig polyclonal Anti-VGLUT1	Millipore	Cat #AB5905; RRID: AB_2301751
Mouse monoclonal Anti-Gephyrin	Synaptic Systems	Cat #147 011; RRID: AB_887717
Mouse monoclonal Anti-PSD-95	NeuroMab	Cat #75-028; RRID: AB_2292909
Mouse monoclonal Anti-β-Actin	Santa Cruz Biotechnology	Cat #sc-47778; RRID: AB_626632
Rabbit polyclonal Anti-$GABA_AR\gamma 2$	Synaptic Systems	Cat #224 003; RRID: AB_2263066
Mouse monoclonal Anti-Gephyrin	Synaptic Systems	Cat #147 111; RRID: RRID: AB_887719
Mouse monoclonal Anti-Synaptophysin	Sigma-Aldrich	Cat #S5768; RRID: AB_477523
Mouse monoclonal Anti-CASK	NeuroMab	Cat #75-000; RRID: AB_2068730
Mouse monoclonal Anti-GluN1	Millipore	Cat #MAB363; RRID: AB_94946
Rabbit polyclonal Anti-Cav2.1	Synaptic systems	Cat #152 203; RRID: AB_2619841
Rabbit polyclonal anti-RIM1/2	Synaptic Systems	Cat #140 203; RRID: AB_887775
Rabbit polyclonal anti-Munc 13-1	Synaptic systems	Cat #126 103; RRID: AB_887733
Mouse monoclonal anti-ELKS	Sigma-Aldrich	Cat #E4531; AB_2100013
Rabbit polyclonal anti-GluA1	Kim et al., 2009	1193; RRID:AB_2722772
Rabbit polyclonal anti-GluA2	Kim et al., 2009	1195; RRID: AB_2722773
Rabbit polyclonal anti-pan-Shank	Kim et al., 2009	1172; RRID: AB_2810261
Rabbit polyclonal anti-Homer	Lie et al., 2016	1133; RRID: AB_2810985
Rabbit polyclonal anti-RIM-BP2	Synaptic systems	Cat #316 103; RRID: AB_2619739
Rabbit polyclonal anti-Liprin-α2	Han et al., 2018	RRID: AB_2810258
Rabbit polyclonal anti-Liprin-α3	Han et al., 2018	RRID: AB_2810259

Mouse monoclonal anti-Syntaxin	Synaptic systems	Cat # 110 011; RRID: AB_887844
Mouse monoclonal anti-Bassoon	Enzo Life Sciences	Cat # SAP7F407; RRID: AB_2313990
Rabbit polyclonal anti-GluN2A	Millipore	Cat # 07-632; RRID: AB_1121300
Mouse monoclonal anti-NeuN	Millipore	Cat # MAB377; RRID: AB_177621
Chicken polyclonal anti-Tbr1	Millipore	Cat # AB2261; RRID: AB_10615497
Rabbit polyclonal anti-Wfs1	Proteintech	Cat # 11558-1-AP RRID: AB_2216046
Rabbit polyclonal Anti-MAP2	Abcam	Cat # ab32454; RRID: AB_776174
Mouse monoclonal Anti-MAP2	Sigma-Aldrich	Cat # M1406; RRID: AB_477171
Cy3 conjugated Donkey Anti-Mouse	Jackson ImmunoResearch Laboratories	Cat #715-165-150; RRID: AB_2340813
Cy3 conjugated Donkey Anti-Rabbit	Jackson ImmunoResearch Laboratories	Cat #711-165-152; RRID: AB_2307443
Cy3 conjugated Donkey Anti-Guinea pig	Jackson ImmunoResearch Laboratories	Cat #706-165-148; RRID: AB_2340460
FITC conjugated Donkey Anti-Mouse	Jackson ImmunoResearch Laboratories	Cat #715-035-150; RRID: AB_2340770
FITC conjugated Donkey Anti-Rabbit	Jackson ImmunoResearch Laboratories	Cat #711-095-152; RRID: AB_2315776
FITC conjugated Donkey Anti-Chicken	Jackson ImmunoResearch Laboratories	Cat #703-095-155; RRID: AB_2340356
Chemicals, Peptides, and Recombinant Proteins		
Lipofectamine LTX Reagent with PLUS™ Reagent	ThermoFisher Scientific	Cat #15338100
Neurobasal medium	ThermoFisher Scientific	Cat #21103049
B-27 supplement (50X)	ThermoFisher Scientific	Cat #17504-044

Penicillin/Streptomycin	ThermoFisher Scientific	Cat #15140122
HBSS (Hanks' Balanced Salt Solution)	ThermoFisher	Cat #14065056
GlutaMax Supplement	ThermoFisher Scientific	Cat #35050061
Fetal Bovine Serum (FBS)	WELGENE	Cat #PK004-01
Sodium pyruvate	ThermoFisher Scientific	Cat #11360070
Poly-D-lysine hydrobromide	Sigma-Aldrich	Cat #P0899
Glutaraldehyde solution	Sigma-Aldrich	Cat #G5882
Sodium cacodylate trihydrate	Sigma-Aldrich	Cat #C4945
2,2,2-Tribromoethanol (Avertin)	Sigma	Cat #T48402
Ethanol	Millipore	Cat #1.00983.1011
Vectashield mounting medium	Vector Laboratories	Cat #H-1200
6-Cyano-7-nitroquinoxaline-2,3-dione (CNQX)	Sigma-Aldrich	Cat #C127
2,3-Dioxo-6-nitro-1,2,3,4-tetrahydrobenzo (NBQX)	Hello Bio	Cat #HB0443
Tetrodotoxin (TTX)	Tocris	Cat #1069
Bicuculline	Tocris	Cat #0130
Picrotoxin	Tocris	Cat #1128
QX-314	Tocris	Cat #1014
D-2-amino-5-phosphonovalerate (D-AP5)	Tocris	Cat #0106
Critical Commercial Assays		
ReverTra Ace-α Kit	Toyobo	Cat #FSQ-301
CalPhos Transfection Kit	Takara	Cat #631312
Experimental Models: Cell Lines		
HEK 293T cells	ATCC	Cat # CRL-3216
Cultured neurons (from mouse embryos)	N/A	N/A
Experimental Models: Organisms/Strains		

Mouse: *PTPσ* $^{f/f}$	KOMP Repository Collection	N/A
Mouse: *Wfs1-cre*	Kitamura et al., 2014	N/A
Mouse: *Nestin-cre*	The Jackson Laboratory	Cat #003771
Mouse: *Ai9 reporter*	The Jackson Laboratory	Cat #007909
Recombinant DNA		
pAAV-hSyn-ΔCre-GFP	Xu and Südhof, 2013	N/A
pAAV-hSyn-Cre-GFP	Xu and Südhof, 2013	N/A
FSW-ΔCre	Ko et al., 2011	N/A
FSW-Cre	Ko et al., 2011	N/A
L-313 PTPσ WT	Han et al., 2018	N/A
L-313 PTPσ C1157S	Han et al., 2018	N/A
L-313 PTPσ ΔD2	Han et al., 2018	N/A
pCAGG-VGLUT1-Venus	This study	N/A
Sequence-Based Reagents		
Ptprs mouse probe (for qRT-PCR)	This study	N/A
Ptprd mouse probe (for qRT-PCR)	This study	N/A
Ptprf mouse probe (for qRT-PCR)	This study	N/A
Software and Algorithms		
MetaMorph	Molecular Devices	https://www.moleculardevices.com
ImageJ	NIH	https://imagej.nih.gov/ij/
GraphPad Prism 8.0	GraphPad	https://www.graphpad.com
Clampfit 10.5	Molecular Devices	https://www.moleculardevices.com
AxoGraph	AxoGraph Scientific	https://axograph.com/

EXPERIMENTAL MODEL AND SUBJECT DETAILS

Cell Culture

HEK293T cells were cultured in Dulbecco's Modified Eagle's Medium (DMEM; WELGENE) supplemented with 10% fetal bovine serum (FBS; WELGENE) and 1% penicillin-streptomycin (Thermo Fisher) at 37°C in a humidified 5% CO_2 atmosphere. Cultured primary hippocampal neurons were prepared from embryonic day 17 (E17) *PTPσ*$^{f/f}$ mice.

Animals

The use and care of animals complied with the guidelines and protocols (DGIST-IACUC-17122104-01) for rodent experimentation approved by the Institutional Animal Care and Use Committee of DGIST under standard, temperature-controlled laboratory conditions. PTPσ conditional knockout mice were purchased from The KOMP Repository Collection (UC Davis, USA). Ai9 reporter mice were purchased from Jackson Research Laboratories (007909). Nestin-Cre (003771, Jackson Research Laboratories) mice were the gift of Dr. Albert Chen (DUKE-NUS, Singapore). Wfs1-Cre mice were the gift of Dr. Susumu Tonegawa (Massachusetts Institute of Technology, USA). Mice were kept on a 12:12 light/dark cycle (lights on at 9:00 am), and received water and food *ad libitum.* Floxed PTPσ (*PTPσ*$^{f/f}$) were generated by flanking exon 4 with loxP sites (See **Figs. S1** for details). Nestin-Cre driver line was crossed with *PTPσ*$^{f/f}$ mice to generate pan-neuronal PTPσ knockout. Wfs1-Cre driver line was crossed with PTPσ$^{f/f}$ mice to generate mPFC and CA1-specific knockout. Mice were maintained in the C57BL/6N background. Breeding cages are maintained by crossing male PTPσ$^{f/f}$ with female PTPσ$^{f/+}$::Nestin HET (generated by crossing PTPσ$^{f/WT}$ with heterozygous Nestin-Cre transgenic mice), or male *PTPσ*$^{f/f}$ with female *PTPσ*$^{f/f}$::Wfs1 HET (generated by crossing *PTPσ*$^{f/f}$ with heterozygous Wfs1-Cre transgenic mice) mice. All experimental procedures were performed on male mice, using

littermate control without Cre expression.

METHOD DETAILS

Construction of Expression Vectors. *1. PTPσ rescue constructs.* The lentiviral PTPσ rescue vectors were previously described (Han et al., 2018). *2. Others*. The plasmids pAAV-hSyn-ΔCre-GFP and pAAV-hSyn-Cre-GFP were from Dr. Thomas C. Südhof (Stanford University, Palo Alto, CA, USA); FSW-ΔCre and FSW-Cre were from Dr. Pascal S. Kaeser (Harvard University, Cambridge, MA, USA); and pCAGG-VGLUT1-Venus was from Dr. Franck Polluex (Columbia University, New York, NY, USA).

Antibodies. Commercially obtained antibodies included: mouse monoclonal anti-GAD67 (clone 1G10.2; Millipore; RRID: AB_2278725), guinea pig polyclonal anti-VGLUT1 (Millipore; RRID: AB_2301751), rabbit polyclonal anti-VGLUT1 (Synaptic Systems; RRID: AB_887880), rabbit polyclonal anti-$GABA_AR\gamma2$ (Synaptic Systems; RRID: AB_2263066), mouse monoclonal anti-PSD-95 (clone K28/43; Neuromab; RRID: AB_2292909), mouse monoclonal anti-PTPσ (clone 17G7.2; MediMabs; RRID: AB_1808357), mouse monoclonal anti-CASK (clone K56A/50; NeuroMab; RRID: AB_2068730), mouse monoclonal anti-HA (clone 16B12; BioLegend; RRID: AB_2565006); mouse monoclonal anti-Bassoon (clone SAP7F407; Enzo Life Sciences; RRID: AB_2313990), mouse monoclonal anti-Syntaxin (clone SAP7F407; Enzo Life Sciences; RRID: AB_887844), mouse monoclonal anti-NeuN (clone A60; Millipore; RRID: AB_177621), chicken polyclonal anti-Tbr1 (Millipore; RRID: AB_177621), rabbit polyclonal anti-Wfs1 (Proteintech; AB_2216046), goat polyclonal anti-GFP (Rockland; AB_218182), rabbit polyclonal anti-GluN2A (Millipore; AB_11213002), rabbit polyclonal anti-Munc13-1 (Synaptic Systems; RRID: AB_887733), rabbit polyclonal anti-RIM-BP2 (Synaptic Systems; RRID: AB_2619739), rabbit

polyclonal anti-RIM1/2 (Synaptic Systems; RRID: AB_887775), mouse monoclonal anti-ELKS (Sigma-Aldrich; RRID: AB_2100013), mouse monoclonal anti-Synaptophysin (clone SVP-38; Sigma-Aldrich; RRID: AB_477523), mouse monoclonal anti-MAP2 (clone AP-20; Sigma-Aldrich; RRID: AB_477171), rabbit polyclonal anti-MAP2 (Abcam; RRID: AB_776174), mouse monoclonal anti-β-actin (clone C4; Santa Cruz Biotechnology; RRID: AB_626632), mouse monoclonal GluN1 (clone 54.1; Millipore; RRID: AB_94946), rabbit polyclonal Cav2.1 (Synaptic Systems; RRID: AB_2619841), and mouse monoclonal anti-Gephyrin (clone 3B11; Synaptic Systems; RRID: AB_887717). Rabbit polyclonal anti-liprin-α2 (RRID:AB_2810258) and rabbit polyclonal anti-liprin-α3 (RRID:AB_2810259) antibodies were gifts of Dr. Susanne Schoch-McGovern (Bonn, Germany); rabbit polyclonal anti-pan-Shank (1172; RRID: AB_2810261), rabbit polyclonal anti-GluA1 (1193; RRID: AB_2722772), rabbit polyclonal anti-GluA2 (1195; RRID: AB_2722773), and rabbit polyclonal anti-Homer1 antibodies (1133; RRID: AB_2810985) were the gifts of Dr. Eunjoon Kim (KAIST, Korea).

Chemicals. 6-Cyano-7-nitroquinoxaline-2,3-dione (CNQX) was obtained from Sigma-Aldrich (Cat No. C127). Tetrodotoxin (TTX; Cat No. 1069); picrotoxin (Cat No. 1128), QX-314 (Cat No. 1014); and D-2-amino-5-phosphonovalerate (D-AP5; Cat No. 0106) were purchased from Tocris.

Neuron Culture, Transfections, Imaging, and Quantitation. Hippocampal and cortical mouse neuron cultures were prepared from embryonic day 17 (E1) mouse embryos, as described previously (Ko et al., 2011). Mouse cultured neurons were seeded onto coverslips coated with poly-D-lysine (Sigma-Aldrich), and grown in Neurobasal medium supplemented with B-27 (Thermo Fisher), 0.5% FBS (WELGENE), 0.5 mM GlutaMAX (Thermo Fisher), and sodium pyruvate (Thermo Fisher). Cultured neurons (mostly excitatory neurons) were infected with lentiviruses at DIV3–4. For

immunocytochemistry, cultured neurons were fixed with 4% paraformaldehyde/4% sucrose in PBS for 10–30 min at 4°C, and permeabilized with 0.2% Triton X-100 in PBS for 10–30 min at 4°C. Neurons were blocked with 3% horse serum/0.1% BSA in PBS for 15 min at room temperature and incubated with primary and secondary antibodies in blocking solution for 70 min at room temperature. The primary antibodies were used in these experiments included anti-VGLUT1 (Synaptic Systems; 1:700), anti-GAD67 (Millipore; 1:100), anti-$GABA_AR\gamma2$ (Synaptic Systems; 1:500), anti-GluA1 (1193; 1:200), anti-Gephyrin (Synaptic Systems; 1:100), and anti-pan-Shank (1172; 1:200). Images of randomly selected neurons were acquired using a confocal microscope (LSM800, Carl Zeiss) with a 63 × objective lens; all image settings were kept constant during image acquisition. Z-stack images obtained by confocal microscopy were converted to maximal projections, and puncta size and the density of the indicated presynaptic marker proteins were analyzed in a blinded manner using MetaMorph software (Molecular Devices Corp.).

Production of Lentiviruses. Lentiviruses were produced by transfecting HEK293T cells with three plasmids—lentivirus vectors, psPAX2, and pMD2.G—at a 2:2:1 ratio. After 72 h, lentiviruses were harvested by collecting the media as previously described (Han et al., 2018; Hsia et al., 2014).

Production of Adeno-associated Viruses. HEK293T cells were co-transfected with the indicated AAV vectors, pHelper and AAV1.0 (serotype 2/9) capsids vectors. After 72 hours, the transfected HEK293T cells were collected, and resuspended in PBS, and lysed by subjecting them to four freeze-thaw cycles in an ethanol/dry ice bath (7 minutes each) and a 37°C water bath (5 min). The lysates were centrifuged and the supernatants were mixed with 40% polyethylene glycol and 2.5 M NaCl and centrifuged at 2000 × g for 30 min. The cell pellets were resuspended in HEPES buffer (20 mM HEPES, 115 mM NaCl, 1.2 mM $CaCl_2$, 1.2 mM $MgCl_2$, and 2.4 mM KH_2PO_4, pH 8.0) to which was added an equal volume of chloroform. The mixture was centrifuged at 400 × g for 5 min and concentrated

three times with a Centriprep centrifugal filter (Cat. 4310, Millipore) at 1,220 × g (20 min each) and an Amicon Ultra centrifugal filter (Cat. UFC500396, Millipore) at 16,000 × g for 30 min. AAVs were titered by treating 1 µl of concentrated, filter-sterilized AAVs with 1 µl of DNase I (AMPD1; Sigma) for 30 min at 37 °C to eliminate any contaminating plasmid DNA. After treatment with 1 µl of stop solution (50 mM ethylenediaminetetraacetic acid) for 10 min at 65 °C, 10 µg of protease K (Cat. P2308; Sigma) was added and the sample was incubated for 1 h at 50°C. Reactions were stopped by heat inactivation at 95 °C for 20 min. The final virus titer was quantified by qRT-PCR. Empty AAV vector was used to generate a standard curve for qRT-PCRs targeting *GFP* sequences.

qRT-PCRs. Cultured rat cortical neurons were infected with recombinant lentiviruses at DIV4 and harvested at DIV13 for qRT-PCR using SYBR green qPCR master mix (TaKaRa). Total RNA was extracted from mouse cortical neurons using TRIzol reagent (Invitrogen) according to the manufacturer's protocol. Briefly, cells in each well of a 12-well plate of cultured neurons were harvested and incubated with 500 µl TRIzol reagent at room temperature for 5 minutes. After phenol-chloroform extraction, RNA in the upper aqueous phase was precipitated. cDNA was synthesized from 500 ng of RNA by reverse transcription using a ReverTra Ace-α kit (Toyobo). Quantitative PCR was performed on a CFX96 Touch Real-Time PCR system BioRad) using 0.5 µl of cDNA. The ubiquitously expressed β-actin was used as an endogenous control. The sequences of the primer pairs used were: mouse *Ptprs*, 5'-ATCAGAGAGCCCAAGGATCA-3' (forward) and 5'-GCCACACACTCGTACACGTT-3' (reverse); mouse *Ptprd*, 5'-CTCCTTGATCCCCATCTCTG–3' (forward) and 5'-CAG GGCAGCCACTAAACTTC-3' (reverse); and mouse *Ptprf*, 5'- CCCGATGGCTGAGTACAACA-3' (forward) and 5'-CATCCCGGGCGTCTGTGA-3' (reverse).

Electron Microscopy. E17 embryonic hippocampi of *PTPσ*$^{f/f}$ mice were seeded onto 18 mm coverslips at densities of 40,000 cells/well. The neurons were infected with lentiviral vectors expressing ΔCre or

Cre at DIV4. At DIV14, cultured neurons were fixed in 2% glutaraldehyde, 0.1 M Na-cacodylate buffer, pH 7.4, for 1 h at room temperature and overnight at 4°C. The cells were post-fixed in 0.5% OsO4 (osmium tetroxide), 0.8% K ferricyanide at room temperature for 60 min. All specimens were stained *en bloc* with 2% aqueous uranyl acetate for 30 min, dehydrated in a graded ethanol series up to 100%, embedded in Embed 812 resin (Electron Microscopy Science, PA), and polymerized overnight in a 60 °C oven. Thin sections (50–60 nm) were cut with a Leica ultramicrotome and post-stained with uranyl acetate and lead citrate. Sample grids were examined using a FEI Tecnai BioTWIN transmission electron microscope running at accelerating voltage of 80 kV. Images were recorded with a Morada CCD camera and iTEM (Olympus) software. This protocol allowed the unambiguous staining of membranes of synaptic vesicles as well as of pre- and post-synaptic compartments, resulting in accurate measurements of the nanoscale organization of the synaptic vesicles within nerve endings. To analyze synapse ultrastructure, the lengths of active zone and PSD, tethered vesicles, the membrane proximal vesicles, and total vesicle numbers were quantified using MetaMorph software (Molecular Devices Corp.). The numbers of total vesicles and docked vesicles were counted manually, and the distances from the active zone and the PSD to the vesicle center were measured. Vesicles located below 200 nm were considered membrane-proximal vesicles.

RNAscope Analyses. RNAscope analyses of mouse brains were performed using RNAscope® Fluorescent Multiplex Assay kits (Advanced Cell Diagnostics) according to the manufacturer's direction. Briefly, within 5 min of dissection, mouse brains were immersed in cryo-embedding medium and frozen on dry ice. Brain tissue was sliced into 20 µm-thick coronal sections using a cryotome (Model CM-3050-S; Leica Biosystems), mounted, and dried at –20°C for 10 min. Tissue samples were fixed with 4% formaldehyde for 15 minutes at 4°C and dehydrated by incubation at room temperatures (RT) in 50% EtOH for 5 min, in 70% EtOH for 5 min, and twice 100% EtOH for 5 min. The fixed samples were treated with protease IV for 30 min at RT and

washed twice with 1X PBS. To detect RNA, the sections were incubated in different amplifier solutions in a HybEZ hybridization oven (Advanced Cell Diagnostics) at 40°C. Three synthetic oligonucleotides complementary to nucleotide residues 1051–1947 of Mm–*Ptprs*–C1, 1329–2486 of Mm-*Ptprd*–C1 and Mm-*Ptprd*–C2, and 4001–5386 of Mm–*Ptprf*-C3 (Advanced Cell Diagnostics) were labeled by conjugation to Alexa Fluor 488, Altto 550 and Altto 647, and the labeled probe mixtures were hybridized by tissue samples by incubating them with slide-mounted sections for 2 hours at 40°C. Nonspecifically hybridized probes were removed by washing the sections three times for 2 minutes each with 1X wash buffer at RT, followed by incubations at 40°C with Amplifier 1-FL for 30 minutes, Amplifier 2-FL for 15 minutes, Amplifier 3-FL for 30 minutes, and Amplifier 4 Alt B-FL for 15 minutes. Each amplifier was removed by washing twice in 1X wash buffer at RT. The fluorescence images were acquired using a LSM 800 microscope (Carl Zeiss).

Stereotaxic Surgery and Virus Injections. 6–7-week-old mice were anesthetized by intraperitoneal injection of 2% 2,2,2-tribromoethanol (Sigma), dissolved in saline, and secured in a stereotaxic apparatus. Viral solutions were injected using a Nanoliter 2010 Injector (World Precision Instruments), including a NanoFil syringe and 33 gauge needle, at a flow rate of 50 nl/min (injected volume, 500 nl). The coordinates used for stereotaxic injections targeting the ventral hippocampal CA1 were, relative to the bregma, anteroposterior (AP) -3.1 mm; medial–lateral (ML), ± 3.2 mm; and dorsal–ventral (DV), -2.5 mm. Immunohistochemical analyses were performed 3 weeks later.

Immunohistochemistry. Male mice aged 8–10-weeks were anesthetized and immediately perfused, first with PBS for 5 minutes and then with 4% paraformaldehyde for 5 minutes. Their brains were removed, fixed overnight in 4% paraformaldehyde, incubated overnight in 30% sucrose (in PBS), and

sliced into 35-µm-thick coronal sections using a cryotome (Model CM-3050-S; Leica Biosystems). The sections were permeabilized in PBS containing 0.5% Triton X-100 for 1 h and blocked in PBS containing 5% bovine serum albumen and 5% horse serum for 1 minutes. The brain sections were incubated overnight with primary antibodies for overnight at 4 °C. The following primary antibodies were used: anti-VGLUT1 (1:200), anti-GAD67 (1:100). The brain sections were washed three times with PBS and incubated with the appropriate Cy3-conjugated secondary antibodies (Jackson ImmunoResearch) for 2 hours at RT. After three washes with PBS, the sections were counterstained with DAPI (4',6-diamidino-2-phenylinodole) and mounted onto glass slides (Superfrost Plus; Fisher Scientific) with Vectashield mounting medium (H-1200; Vector Laboratories).

In Vitro **and** ***Ex Vivo*** **Electrophysiology.** *1. Electrophysiology of Primary Cultured Neurons.* Hippocampal neurons obtained from PTPσ cKO mice were infected on DIV4 with lentiviruses encoding Cre-EGFP or dCre-EGFP, followed by analysis at DIV13-16. Pipettes were pulled from borosilicate glass (o.d. 1.5 mm, i.d. 0.86 mm; Sutter Instrument), using a Model P-97 pipette puller (Sutter Instrument). The resistance of pipettes filled with internal solution varied between 3-6 MΩ. The internal solution (in mM) contained 145 CsCl, 5 NaCl, 10 HEPES, 10 EGTA, 0.3 Na-GTP, and 4 Mg-ATP with pH adjusted to 7.2–7.4 with CsOH, and an osmolarity of 290–295 mOsmol/L. The external solution (in mM) consisted of 130 NaCl, 4 KCl, 2 $CaCl_2$, 1 $MgCl_2$, 10 HEPES, and 10 D-glucose with pH adjusted to 7.2–7.4 with NaOH, and an osmolarity of 300–305 mOsmol/L. Whole-cell configuration was generated at RT using MPC-200 manipulators (Sutter Instrument) and a Multiclamp 700B amplifier (Molecular Devices). mEPSCs, mIPSCs, and sucrose EPSCs were recorded at a holding potential of -70 mV. For sucrose puffing, 500 mM sucrose was applied directly on the dendritic field of the patched neurons at a puff pressure of 6–8 psi using a PV-820 Pneumatic Picopump system (World Precision Instruments). Receptor-mediated synaptic responses were pharmacologically isolated by applying drug

combinations of 50 μM picrotoxin, 10 μM CNQX, 50 μM D-APV and/or 1 μM tetrodotoxin. Synaptic currents were analyzed offline using Clampfit 10.5 (Molecular Devices) software. *2. Acute Slice Electrophysiology*. Transverse hippocampal formation (300 μm) were prepared from 10–12-week-old male mice, as described (Noh et al., 2019). The mice were anesthetized with isoflurane and decapitated, and their brains were rapidly removed and placed in ice-cold, oxygenated (95% O_2/5% CO_2), low-Ca^{2+}/high-Mg^{2+} dissection buffer (in mM) containing 5 KCl, 1.23 NaH_2PO_4, 26 $NaHCO_3$, 10 dextrose, 0.5 $CaCl_2$, 10 $MgCl_2$, and 212.7 sucrose. Slices were transferred to a holding chamber in an incubator containing oxygenated (95% O_2/5% CO_2) artificial cerebrospinal fluid (ACSF in mM) containing 124 NaCl, 5 KCl, 1.23 NaH_2PO_4, 2.5 $CaCl_2$, 1.5 $MgCl_2$, 26 $NaHCO_3$, and 10 dextrose at 28–30°C for at least 1 h before recording. After > 1 h incubation in ACSF, slices were transferred to a recording chamber with continuous perfusion (2 ml/min) by ACSF oxygenated with 95% O_2/5% CO_2 at 23–25°C. All recordings were performed on pyramidal neurons in the subiculum or hippocampal CA1 area identified by their size and morphology. Patch pipettes (4–6 MΩ) were filled with a solution (in mM) containing 130 Cs-$MeSO_4$, 0.5 EGTA, 5 TEA-Cl, 8 NaCl, 10 HEPES, 1 QX-314, 4 ATP-Mg, 0.4 GTP-Na, and 10 phosphocreatine-Na_2 to record mEPSCs and AMPA/NMDA ratio; 135 K-gluconate, 8 NaCl, 10 HEPES, 2 ATP-Na and 0.2 GTP-Na to record sEPSCs and eEPSC-PPRs with pH 7.4 and an osmolarity of 280–290 mOsmol/L. The extracellular recording solution consisted of ACSF supplemented with picrotoxin (100 μM) for sEPSCs, and with TTX (1 μM), DL-AP5 (50 μM), and picrotoxin (100 μM) for measuring mEPSCs. Evoked synaptic responses were elicited by stimulation (0.2 ms current pulses) using a concentric bipolar electrode placed 200–300 mm in front of postsynaptic pyramidal neurons at intensities that produced 40–50% of the maximal EPSC amplitude. Recordings were obtained using a Multiclamp 700B amplifier (Molecular Devices) under visual control with differential interference contrast illumination on an upright microscope (BX51WI; Olympus). Data were acquired and analyzed using pClamp 10.7

(Molecular Devices). Signals were filtered at 3 kHz and digitized at 10 kHz with DigiData 1550 (Molecular Devices).

QUANTIFICATION AND STATISTICAL ANALYSIS

Data Analysis and Statistics. All data are expressed as means ± SEM. All experiments were repeated using at least three independent cultures, and data were statistically evaluated using a Mann-Whitney *U* test, analysis of variance (ANOVA) followed by Tukey's *post hoc* test, Kruskal-Wallis test (one-way ANOVA on ranks), paired two-tailed t-test (for electrophysiology experiments), or one-way ANOVA with Bonferroni's *post hoc* test (for behavior experiments), as appropriate. Prism8 (GraphPad Software) was used for analysis of data and preparation of bar graphs. *P* values < 0.05 were considered statistically significant (individual *p* values are presented in figure legends).

SUPPLEMENTAL REFERENCES

Han, K.A., Ko, J.S., Pramanik, G., Kim, J.Y., Tabuchi, K., Um, J.W., and Ko, J. (2018). PTPsigma Drives Excitatory Presynaptic Assembly via Various Extracellular and Intracellular Mechanisms. J. Neurosci. 38, 6700-6721.

Hsia, H.E., Kumar, R., Luca, R., Takeda, M., Courchet, J., Nakashima, J., Wu, S., Goebbels, S., An, W., Eickholt, B.J.*, et al.* (2014). Ubiquitin E3 ligase Nedd4-1 acts as a downstream target of PI3K/PTEN-mTORC1 signaling to promote neurite growth. Proc. Natl. Acad. Sci. U S A 111, 13205-13210.

Kim, M.H., Choi, J., Yang, J., Chung, W., Kim, J.H., Paik, S.K., Kim, K., Han, S., Won, H., Bae, Y.S.*, et al.* (2009). Enhanced NMDA receptor-mediated synaptic transmission, enhanced long-term potentiation, and impaired learning and memory in mice lacking IRSp53. J. Neurosci. 29, 1586-1595.

Kitamura, T., Pignatelli, M., Suh, J., Kohara, K., Yoshiki, A., Abe, K., and Tonegawa, S. (2014). Island cells control temporal association memory. Science 343, 896-901.

Ko, J., Soler-Llavina, G.J., Fuccillo, M.V., Malenka, R.C., and Südhof, T.C. (2011). Neuroligins/LRRTMs prevent activity- and Ca2+/calmodulin-dependent synapse elimination in cultured neurons. J. Cell Biol. 194, 323-334.

Lie, E., Ko, J.S., Choi, S.Y., Roh, J.D., Cho, Y.S., Noh, R., Kim, D., Li, Y., Kang, H., Choi, T.Y.*, et al.* (2016). SALM4 suppresses excitatory synapse development by cis-inhibiting trans-synaptic SALM3-LAR adhesion. Nat. Commun. 7, 12328.

Noh, K., Lee, H., Choi, T.Y., Joo, Y., Kim, S.J., Kim, H., Kim, J.Y., Jahng, J.W., Lee, S., Choi, S.Y., and Lee, S.J. (2019). Negr1 controls adult hippocampal neurogenesis and affective behaviors. Mol. Psychiatry 24, 1189-1205.

Xu, W., and Südhof, T.C. (2013). A neural circuit for memory specificity and generalization. Science 339, 1290-1295.